Author Manuscript

Author Manuscript

Author Manuscript

Author Manuscript

HHS Public Access

Author manuscript

Nat Neurosci. Author manuscript; available in PMC 2023 January 06.

Published in final edited form as:

Nat Neurosci. 2022 August ; 25(8): 1059–1070. doi:10.1038/s41593-022-01102-9.

Memory-enhancing properties of sleep depend on the oscillatory amplitude of norepinephrine

Celia Kjaerby[1,†,*], **Mie Andersen**[1,†], **Natalie Hauglund**[1], **Verena Untiet**[1], **Camilla Dall**[1], **Björn Sigurdsson**[1], **Fengfei Ding**[2,3], **Jiesi Feng**[4], **Yulong Li**[4,5,6], **Pia Weikop**[1], **Hajime Hirase**[1], **Maiken Nedergaard**[1,2,*]

[1]Division of Glial Disease and Therapeutics, Center for Translational Neuromedicine, University of Copenhagen, 2200 Copenhagen, Denmark.

[2]Division of Glial Disease and Therapeutics, Center for Translational Neuromedicine, Department of Neurosurgery, University of Rochester Medical Center, Rochester, NY 14642, USA.

[3]Department of Pharmacology, Shanghai Medical College, Fudan University, Shanghai, 200032, China

[4]State Key Laboratory of Membrane Biology, Peking University School of Life Sciences, Beijing 100871, China.

[5]PKU-IDG/McGovern Institute for Brain Research, Beijing 100871, China.

[6]Peking-Tsinghua Center for Life Sciences, Academy for Advanced Interdisciplinary Studies, Peking University, Beijing 100871, China.

Abstract

Sleep has a complex microarchitecture, encompassing micro-arousals, sleep spindles, and transitions between sleep stages. Fragmented sleep impairs memory consolidation, whereas spindle- and delta-rich NREM sleep and REM sleep promote it. Yet, the relationship between micro-arousals and memory-promoting aspects of sleep remains unclear. We here use fiber photometry in mice to examine how release of the arousal mediator, norepinephrine (NE), shapes sleep microarchitecture. We show that micro-arousals are generated in a periodic pattern during NREM sleep, riding on the peak of locus coeruleus-generated infraslow oscillations of extracellular NE, whereas descending phases of NE oscillations drive spindles. The amplitude of NE oscillations is crucial for shaping sleep microarchitecture related to memory performance: prolonged descent of NE promotes spindle-enriched intermediate state and REM sleep but also

[*]Corresponding authors: Maiken Nedergaard (nedergaard@sund.ku.dk); Celia Kjaerby (celia.kjaerby@sund.ku.dk).
[†]Authors contributed equally

Author contributions:
Conceptualization: CK, MA, HH, MN, PW
Fiber photometry and EEG Methodology and investigation: CK, MA, NH, CD, VU
Viral constructs: YL, JF, FD
HPLC Methodology: PW
Analysis: CK, MA, BS
Visualization: CK, MA
Supervision: HH, MN
Writing—original draft: CK, MA
Writing—review & editing: CK, MA, HH, MN

Competing interests: Authors declare that they have no competing interests.

Author Manuscript Author Manuscript Author Manuscript Author Manuscript

associates with awakenings, whereas shorter NE descents uphold NREM sleep and micro-arousals. Thus, the NE oscillatory amplitude may be a target for improving sleep in sleep disorders.

Ample research has documented a rich microstructural organization of sleep, based on EEG activity patterns. For instance, NREM sleep encompasses both delta-dominated and spindle-rich epochs[1], the latter characterized by frequent appearances of sigma oscillations (8-15 Hz) bursts. Spindles are thought to play a role in post-sleep performance through the promotion of memory consolidation processes[1,2] and often increase in appearance prior to transition to REM sleep — a phenomenon known as intermediate state (IS) sleep. Uninterrupted sleep is considered important for restorative processes and next-day performance; still, transient arousals known as micro-arousals are increasingly recognized as an intrinsic component of normal sleep microarchitecture[3,4]. External induction of micro-arousals in healthy young subjects worsens performance[5] and conditions associated with frequent micro-arousals such as aging and dementia display spindle reduction and cognitive decline[6-8]. Nonetheless, how micro-arousals and memory-enhancing processes, such as spindles, are interconnected and controlled is unknown.

Sleep–wake transitions are orchestrated by several wake- and sleep-promoting regulatory systems[9], among which the neuromodulator norepinephrine (NE) released from the locus coeruleus (LC) is intimately linked to wakefulness and attention[10-15]. LC activity is strongly reduced during sleep[11,13,14,16,17], and extracellular NE is highest during wake, lower during NREM sleep and lowest during REM sleep[18,19]. Yet, the LC-NE system has not been shown to shape sleep microarchitecture[13,14,16,17,20], although differential LC-NE activity during NREM sleep has been implicated in the termination of sleep spindles[11,21-25]. Spindle activity has been demonstrated to slowly oscillate during NREM sleep[23]. We here tested the hypothesis that oscillatory LC-NE-mediated activity during sleep is responsible for the generation of both micro-arousals and the memory-improving spindle activity. A corollary of this hypothesis is that the oscillatory amplitude of NE, rather than the absolute level, shapes the microarchitecture of sleep.

Until now, technical and temporal constraints of electrochemical and microdialysis-based NE measurements have limited our insight into the dynamics between extracellular NE levels and the microarchitecture of sleep. We took advantage of a fluorescent NE biosensor[26] and population-based LC Ca^{2+} imaging to make high temporal resolution measurements of the LC-NE system and correlate it with the distinct phases of sleep. Our observations reveal that periodic LC activity during NREM sleep drives infraslow (~30 s) extracellular NE oscillations that are responsible for a cyclic pattern of intrinsic micro-arousals, with only a small fraction of the oscillations resulting in awakening. Intriguingly, we demonstrate that the amplitude of NE oscillations tunes the microstructural organization of sleep related to memory performance: the descending phase of NE oscillations drives spindle activity, and increased descent amplitude promotes spindle-rich intermediate state and REM sleep transition. The NE descent amplitude also determines the size of the successive LC activation and the resulting behavioral outcome. Specifically, long NE descents results in large LC activation and full awakenings, while shorter NE descents lead to more subtle LC activation, causing micro-arousals rather than awakenings. Induction of NE descent

Author Manuscript Author Manuscript Author Manuscript Author Manuscript

by LC optogenetic suppression enhances memory performance, whereas pharmacological and optogenetic reduction of NE oscillation amplitude worsens memory performance. In conclusion, we demonstrate a novel and critical role of NE oscillations in shaping sleep microarchitecture and identify manipulations that directly enhance memory-promoting segments of sleep.

Results

Increased NE descent amplitude primes awakenings over micro-arousals

To dissect the role of LC-NE in shaping the microarchitecture of sleep, we combined fiber photometry with EEG and EMG measurements, and correlated real-time LC activity with NE level in medial prefrontal cortex (mPFC) during sleep (Figure 1a-b). LC activity was recorded by imaging of GCaMP6f, which was delivered by AAV injection in TH-Cre transgenic mice, while an improved version of the NE biosensor, $GRAB_{NE2m}$[26], was expressed in mPFC neurons to image NE dynamics (Figure 1a, Suppl. Figure S1). Prior to collection of data, the sensitivity of prefrontal $GRAB_{NE2m}$ towards NE and not dopamine in mPFC was assessed (Suppl. Figure S2).

Continuous recordings covering multiple sleep–wake episodes revealed that a pronounced infraslow oscillatory pattern[24] dominated the mPFC NE dynamics during NREM sleep (Figure 1b-c), which was not observed with an NE-insensitive version of the GRAB sensor (Suppl. Figure S3)[26]. The NE ascends correlated with bursts of LC activity, and NE slowly descended between episodes of LC activity with a periodicity of ~30 s (frequency of 0.034+/−0.004 Hz, Figure 1c-d, Extended Data Figure 1e). The NE oscillations had a mean amplitude of 3.1+/−0.5 % during NREM sleep and 5.2+/−1.1 % during REM sleep, where a continuous NE descent was observed (Figure 1d). We speculated that this non-stationary nature of NE levels provides a novel way of dissecting the complex nature of sleep microarchitecture. The oscillatory NE ascents during NREM sleep were subdivided into those resulting in wakefulness (>15 s, $wake^{EEG/EMG}$) or micro-arousals (<15 s, $MA^{EEG/EMG}$) (Figure 1e). Interestingly, NE ascents that were not accompanied by EMG changes still produced reductions in EEG amplitudes across theta and sigma frequencies (Extended Data Figure 1), which are established EEG-based criteria for micro-arousals[27]. We thus termed these transitions for 'micro-$arousals^{NE}$' (MA^{NE}) (Figure 1e). Only 7.9% of all NE ascends during NREM sleep resulted in awakenings, whereas 29.2% and 63% were associated with $MA^{EEG/EMG}$ and MA^{NE}, respectively (Figure 1f). These observations indicate that intrinsic LC-driven NE fluctuations drive a cyclic pattern of micro-arousals during sleep, while only a minority result in awakenings.

As expected, onset of LC activity bouts preceded NE ascends, and the amplitude of LC responses were highest during $wake^{EEG/EMG}$ and similar between MA^{NE} and $MA^{EEG/EMG}$ transitions (Figure 1g-i). Surprisingly, even though the slope of the NE descent prior to the LC activity bouts were similar across all state transitions (Figure 1j-k), the duration of the descent was longer prior to awakening, resulting in lower NE trough levels prior to awakening compared to micro-arousals (Figure 1l-m). The subsequent NE ascent amplitude and rise time were higher for awakenings compared to micro-arousals (Figure 1n, Extended

Author Manuscript Author Manuscript Author Manuscript Author Manuscript

Data Figure 1c-d), which associated with the higher wake-related LC response amplitude (Figure 1h-i).

Based on the observation of lower NE trough levels prior to awakenings, we wondered if NE level could predict the sensitivity towards arousal input. To test this hypothesis, mice were exposed to auditory stimulations (0.5 s) during sleep (Figure 1o). To include all arousals independently of EMG, we used reductions in EEG sigma power to divide tone outcome into arousal and sustained sleep (Extended Data Figure 2 + Figure 1o), previously validated to be a consistent EEG component of micro-arousals (Extended Data Figure 1). This analysis showed that the NE trough level was lower prior to tones that resulted in arousal compared to those that did not (Figure 1q). Although NE signals during maintained sleep also responded to the tone and reached similar peak values, the amplitude of the NE ascent was lower (Figure 1r). This observation points to the novel concept that NE amplitude, rather than the peak level of NE, determines arousal. To investigate whether the likelihood of tone-induced awakenings could be predicted solely based on the amplitude of the NE descent, we divided trials into high or low NE trough values (above or below mean) prior to the tone. This analysis showed that low NE trough levels were predictive of sound-evoked awakenings during NREM sleep (Figure 1s). In conclusion, we demonstrate that 1) infraslow NE oscillations during NREM sleep coincide with regular micro-arousals suggesting a causal relationship and 2) that larger amplitudes of NE descent increase the likelihood of awakening (Figure 1t).

Prolonged NE descent promotes spindle-rich IS and REM sleep transitions

Next, we investigated how the infraslow NE oscillations shaped the occurrence of sleep spindles. Sleep spindles, characterized as short bursts (1-2 s) of sigma activity (8-15 Hz oscillations), have been implicated in memory consolidation[2], and LC activity has been reported to terminate sleep spindle activity[11,21,22]. First, we confirmed that sigma power – the 8-15 Hz spectral power of surface EEG (5 s windows) – is a good estimate for spindle occurrences (Figure 2a-b). We used cortical local field potential (LFP) recordings to detect spindles and compared it to sigma power obtained from simultaneous EEG recordings. LFP-detected spindle occurrences paralleled EEG sigma power and revealed infraslow sigma power oscillations across NREM sleep (Figure 2a-b, Extended Data Figure 3a-c), with an inverse relationship to the NE oscillations (Figure 2c). Specifically, spindle occurrences (and corresponding sigma power) build up as NE descends and are terminated as NE starts to ascend (Figure 2d, Extended Data Figure 3d). The inverse relationship was also apparent from the peak in sigma power when assessed at times of NE troughs (Figure 2e) and from the NE trough occurring at points of spindle onset (Figure 2f). Spindle onset correlated with a peak in sigma power (Figure 2f), indicating again that sigma power is a good estimate of spindles. Cross-correlation analysis showed a clear inverse correlation between NE and sigma power across the recording (Figure 2g), but causality could not be inferred from the cross-correlogram alone due to the broad peak. We therefore analyzed the temporal relationship between NE level and spindles following optogenetic activation of LC, and demonstrated a time delay between NE ascent and termination of spindles, which further supports the idea that spindle occurrences depend on NE levels (Extended Data Figure 3f). Since delta-rich NREM sleep phases are important for the restorative functions of sleep,

Author Manuscript Author Manuscript Author Manuscript Author Manuscript

we also performed cross-correlation analysis between delta power and NE level, but we did not find an obvious temporal association (Extended Data Figure 3e). In summary, the infraslow oscillations of NE during NREM sleep strongly correlated with a repeated pattern of alternations between sleep spindles and micro-arousals.

Studies have reported LC firing stops during REM sleep[16,28], and interestingly, REM sleep is always preceded by spindle-rich 'intermediate-state' (IS) sleep[29]. Our observations above suggest that IS sleep occurs when the level of NE is already low. However, it is not known whether LC-NE activity is responsible for the transitioning and fixed sequential order of IS and REM sleep. We observed that prior to REM sleep onset, phasic LC events ceased, initiating a continuous descent of NE levels accompanied by spindle build-up that dropped upon REM sleep entry (Figure 2h-i). Remarkably, the NE descent prior to REM sleep started almost 40 s (42.3±3.8 s) before REM sleep onset (Figure 2i and k), suggesting that spindle-rich IS sleep is driven by NE descent. Interestingly, the slope of the NE descent was similar between NREM and IS sleep (Figure 2l), indicating that the subsequent occurrence or absence of a micro-arousal is the main determinant of whether NREM sleep continues or transitions into REM sleep. Furthermore, the overall spindle occurrences (estimated by sigma power) associated with IS sleep was higher than during other phases of NREM sleep (Figure 2l), adding additional support to the importance of IS-to-REM sleep transitions in spindle-dependent memory processes. As expected, NE continued to descend during REM sleep (Figure 2h-i). At the offset of REM sleep, LC exhibited phasic activity accompanied by a rapid ascent in NE (Figure 2j), with a mean delay from onset of NE increase to REM sleep offset of only ~5 s (4.7 ± 0.5 s, Figure 2k). This analysis shows that the sequential order of spindle-rich IS and REM sleep coincide with silence of LC and a continuous descent in cortical NE levels.

Optogenetic LC suppression induces IS-REM sleep sequences and improves memory

To assess the causal role of NE oscillations on memory performance, we sought to increase the amplitude of NE descent in a time-specific manner by periodic optogenetic inhibition. We expressed the light-driven proton pump Arch-eGFP or eYFP-only construct bilaterally in LC TH-positive neurons and delivered continuous green (532-nm, 5 mW in each hemisphere) light to LC for 2 min every 10 min, while recording mPFC $GRAB_{NE2m}$ fluorescence, EEG, and EMG (Figure 3a-b, Extended Data Figure 4a-b). The inhibitory effect of Arch stimulation has been questioned[30], and even though we did not directly assess the effect of Arch stimulation on LC cell firing, we were able to demonstrate a steady descent in NE levels during NREM sleep (Figure 3c-d) following stimulation of Arch-expressing LC cells. The NE descent was accompanied by build-up in sigma power, peaking after ~40 s (Figure 3c-d, Extended Data Figure 4c). The amount of sigma power correlated with the degree of NE descent (Figure 3e). This suggests that low NE plays a permissive role in sleep spindle generation.

Next, we asked if enhancing the amplitude of NE descent would facilitate spindle-rich IS and REM sleep transition. Indeed, optogenetic suppression of LC activity substantially increased the probability of transitioning into REM sleep, with an average delay of 66.1±7.0 s (mean±SEM) from laser stimulation to REM sleep onset (Figure 3f). The ~65 s delay

Author Manuscript Author Manuscript Author Manuscript Author Manuscript

corresponds to the time point when sigma power returns to baseline (Figure 3c) and aligns with the observation that 40 s NE descent precedes REM sleep onset during normal conditions (Figure 2h-k). Additionally, the prolonged elevation of sigma power mimicked sigma increases observed in IS–REM sleep transitions (Extended Data Figure 4d). Thus, these observations suggest that suppression of LC activity and continuous NE descent induces sleep stages similar to the sequentially linked IS and REM sleep.

Next, we examined if the induction of NE descent increased the probability of awakening once LC was released from inhibition. While the rate of micro-arousals decreased during optogenetic suppression of LC (Figure 3g), once the laser was turned off the subsequent NE ascents (Figure 3h-i) were associated with a higher rate of awakenings compared to control animals (Figure 3j), confirming the prior observation that longer periods of NE descent enhance the likelihood of awakening (Figure 1j). However, termination of light-induced Arch stimulation has been associated with rebound excitation activity, which potentially confounds this observation[31,32]. We therefore assessed natural REM sleep incidents, where NE has remained low for an extended period; this revealed that around half of REM sleep offsets are characterized by an awakening, whereas micro-arousals are more prevalent than awakenings at NREM sleep offset (Figure 3k). Thus, enhanced NE descent amplitude may prime the animals towards awakening.

Last, we examined the effects of LC optogenetic suppression on memory performance. The animals were subjected to the novel-object recognition task and afterwards left to sleep between the encoding and recall phase of the task, while stimulated with laser for 2 min every 6 min (Figure 3l). Animals were well habituated to the resting cages and were mainly asleep during the stimulation period, and the majority of stimulations occurred during NREM sleep (Extended Data Figure 4e-f). The stimulations that occurred during wakefulness did not have a significant impact on NE levels or induction of NREM sleep (Extended Data Figure 4g-i). By contrast, suppression of LC increased preference towards the novel objects compared to YFP controls, without affecting the movement of the animal (Figure 3m, Extended Data Figure 4j-k). The preference towards the novel objects correlated strongly with the amount of sigma power induced by the NE suppression (Figure 3n), but not with duration, bout number, or theta power of REM sleep, nor did it correlate with NREM sleep duration or with the amplitude of theta or delta power during laser stimulations Extended Data Figure 4l-q). Thus, enhancing NE descent amplitude by regular LC optogenetic inhibition induces spindle-rich IS-REM sleep sequences and promotes memory performance.

Optogenetic reduction of NE amplitude reduces spindles and disrupts memory performance

To reduce the amplitude of NE oscillations in a sleep-phase specific manner, we performed NE descent-dependent optogenetic activation of LC. We expressed the light-activated cation channel channelrhodopsin-2 (ChR2) bilaterally in TH-positive LC neurons and $GRAB_{NE2m}$ in mPFC neurons, while implanting screws for EEG and EMG measurements (Figure 4a). NE level (ΔF/F (%)) was calculated in real time, and crossing of lower NE threshold values was used to trigger fast optogenetic stimulation of LC (2 s 20 Hz 10 ms blue light pulses).

Author Manuscript Author Manuscript Author Manuscript Author Manuscript

Following habituation, the experiment started with a 2 h baseline recording after which threshold-based activation was initiated and subsequently lifted in increments of 5 ΔF/F (%) every hour (from −15 to 5 ΔF/F (%)) followed by 2 hours of stimulation-free recording (Figure 4a). The stimulation paradigm resulted in a gradual decrease in NE descent amplitude over the cause of the stimulation thresholds (Figure 4b-d) with corresponding reductions in sigma power (Figure 4e-f) and increases in micro-arousal occurrences (Figure 4g). This resulted in an increasingly fragmented NREM sleep pattern (Figure 4h), without affecting the overall duration of NREM sleep (Figure 4i). Of note, REM sleep duration was significantly decreased by LC activation even at low threshold values (Figure 4j).

To investigate if induction of a sleep pattern characterized by low NE oscillatory amplitude and reduced spindle activity would affect memory performance, we again subjected animals to novel-object recognition and stimulated mice with the threshold 0 setting for two hours between memory encoding and recall (Figure 4k). Animals in the ChR2 group did not show a preference for the novel object over the familiar object, unlike animals in the YFP control group, which was not explained by a difference in locomotion during the acquisition or recall phase (Figure 4l-m, Extended Data Figure 5).

Overall, these findings confirm the important role of NE oscillations in shaping sleep micro-architecture important for memory consolidation and suggest that NE amplitude controls the switch between micro-arousal-interspersed NREM sleep and memory-enhancing IS–REM sleep sequences.

Pharmacological reduction of NE amplitude promotes micro-arousals and compromises memory

Our findings suggest that therapeutic treatment based on elevation of NE can lead to altered sleep structure and memory deficits by reducing the amplitude of NE oscillations. Interestingly, antidepressant treatment involving NE reuptake inhibition has been linked to reduced LC responsiveness[33], sedation and REM sleep suppression, but also to sleep disruption[34-36]. To test the postulate that elevated NE will compromise sleep micro-structure through reduced NE dynamics, we administered the NE reuptake inhibitor desipramine (10 mg/kg), and evaluated the impact on sleep starting one hour after administration. Desipramine increased the $GRAB_{NE2m}$ baseline value 20-fold and abolished the infraslow NE oscillatory activity during NREM sleep, as shown by reduced NE oscillation frequency and NE amplitude (Figure 5a-b). Desipramine also altered the sleep pattern (Figure 5c), with increased NREM sleep and total elimination of REM sleep (Figure 5c-d, Extended Data Figure 6a-b). This observation provides support for the permissive effect of NE descent on REM sleep onset, but contradicts the concept that high NE promotes awakening as could be expected from previous literature[15,34,37]. Furthermore, the resulting NREM sleep was characterized by an increased amount of $MA^{EEG/EMG}$ (Figure 5d); intriguingly, however, both $MA^{EEG/EMG}$-induced arousability and $wake^{EEG/EMG}$-induced arousability (defined as reductions in sigma power, Extended Data Figure 1) were substantially decreased and shortened (Figure 5e-g, Extended Data Figure 6c-e). These observations support the idea that NE amplitude rather than absolute NE levels are important for micro-arousal and wake transitioning and that reducing the amplitude of NE oscillations leads to less-defined

Author Manuscript Author Manuscript Author Manuscript Author Manuscript

brain-state transitions. It also corroborates our finding that lower NE descent amplitude primes micro-arousals over awakenings (Figure 1j-l). Furthermore, power spectral analysis revealed reduced EEG power in the sigma and beta range during NREM sleep, but no change in delta and theta bands (Figure 5h-i, Extended Data Figure 6a-b). Reduced sigma power corresponds to a lower occurrence of spindles, suggesting an inverse relationship between NE and spindles. The combination of reduced spindle occurrences and abolished REM sleep transitions suggests that constant elevation of NE compromises spindle-enriched IS-REM sleep transitions. To determine if these sleep changes had any impact on memory performance, a separate batch of mice were given desipramine or saline immediately after the encoding phase of the novel-object recognition task and allowed to sleep for three hours (Figure 5j). During the recall phase, assessing the number of approaches towards the two objects (Figure 5k) revealed that saline-administered animals preferred the novel object, whereas the desipramine-treated animal did not show any preferences (Figure 5l). The movement of the animals during the recall phase was similar as was the movement and object exploration during the drug-free acquisition phase (Extended Data Figure 6f). Thus, desipramine administration reduces the memory performance of the animals without affecting the general activity level of the mice. These results show that drug-induced elevation of NE suppresses sleep micro-structures governed by the infraslow NE oscillations, which compromises memory-promoting segments of sleep.

Taken together, we show that ~0.03 Hz NE oscillations during sleep drive periodic micro-arousals, while longer descents raise the probability of awakening. Increasing oscillation amplitudes allows for increased sleep spindle activity, which supports memory performance and is associated with IS-to-REM sleep transition (Figure 6). By contrast, lowering NE oscillation amplitude by optogenetic or pharmacologic intervention increases micro-arousals and sleep fragmentation, suppresses sleep-spindle activity, and consequently impairs memory performance.

Discussion

It is widely accepted that spindles and REM sleep are important for memory-enhancing aspects of sleep, while excessive fragmentation of sleep negatively impacts daytime performance[5,38,39]. Yet, the neural mechanisms orchestrating naturally occurring sleep-fragmenting elements such as micro-arousals and awakenings and their interrelationship to the memory-enhancing segments of sleep are unknown. Real-time assessment of NE levels by fiber photometry allowed us to dissect the role of NE in sleep microarchitecture with a time resolution of seconds. We found that phasic bouts of LC activity (every ~30 s) during NREM sleep generate infraslow oscillations of cortical NE levels that drive micro-arousals and subdivide sleep into microstructures important for memory consolidation. The analysis reveals that the oscillation amplitude of NE during NREM sleep determines the memory-restorative quality of sleep; reducing or increasing NE oscillatory amplitude either compromises or improves memory performance after sleep. These new observations extend the current view of NE as a neuromodulator that governs macroscale brain states[18,19] to include sleep microarchitecture.

Author Manuscript Author Manuscript Author Manuscript Author Manuscript

The general belief has been that LC reduces its tonic activity during sleep[11,13,14,16,17] with a subsequent overall reduction in NE levels[18,19]. However, we now demonstrate that the NE levels during sleep oscillate in an infraslow manner with a periodicity of ~30 s created by the alternation between LC silence and phasic LC activity. Intriguingly, the LC phasic activity behind the infraslow NE oscillations consistently drives micro-arousals during the NE ascending state. Thus, we unveil a novel mechanism behind spontaneously occurring micro-arousals and demonstrate that micro-arousals are not generated at random during NREM sleep but follow the cyclic nature of LC activations. It is important to note that LC is one of several reciprocally interconnected arousal-promoting systems in the brain that include cholinergic, serotonergic, histaminergic and dopaminergic nuclei collectively known as the ascending reticular activating system[40]. Therefore, it is likely that all these neuromodulators would exhibit increases during micro-arousals; however, our demonstration that optogenetic suppression of LC reduces the appearance of micro-arousals, indicates that LC is particularly important for the initiation of micro-arousals. Since these periodic LC activations during sleep has not been described before, we can only speculate on their origin, but anatomical tracing studies show prominent inputs to LC from medullary nuclei[41,42] indicating a tight connection to the autonomic system[43,44]

After finding that ascending phases of the infraslow NE oscillations drive micro-arousals, we were interested in determining the impact of the descending phase on sleep processes. Previous studies show that the LC-NE system is involved in the termination of sleep spindles; single unit recordings demonstrate that LC firing correlates with the discontinuation of spindles[11,21,22]. We here show that the LC-NE system is also involved in generation of spindles. It is the steady descent of NE that is responsible for build-up of spindles; the amount of NE descent correlates with the amount of spindle activity, and NE ascents abruptly terminate this activity. Thus, the infraslow NE oscillations during NREM sleep drive coherent periodic fluctuations in spindle activity creating distinct spindle-rich sleep structures. The existence of infraslow sigma power fluctuations has been documented in both mice and humans[23], though the primary drive of the oscillations has remained unknown until now[45].

We were interested in determining whether increasing NE oscillatory descent amplitude could increase the amount of spindle build-up during NREM sleep. IS sleep is a well-defined NREM sleep stage that occurs prior to REM sleep onset and is characterized by particularly high spindle activity[46,47].Our analysis demonstrates that the spindle-rich IS sleep is associated with larger descent amplitude of NE compared to remaining NREM sleep. Namely, ~40 s prior to REM sleep, NE starts to descend, which allows enriched build-up of spindle activity. At REM sleep transitioning, spindles are not abruptly terminated, but slowly start to subside likely due to activation of the pedunculopontine nuclei that promotes acetylcholine release and REM sleep transitioning, while suppressing spindle activity through parallel projections to the cholinergic basal forebrain and thalamus[40,48]. The overall induction of spindles is larger for the IS-REM sleep sequence compared to the shorter lasting spindle increases interspersed within NREM sleep.

It is well-established that NE levels are lower during REM sleep than NREM sleep[18,19] and indeed, NE exhibits a continuous descent during REM sleep in addition to the 40 s

Author Manuscript Author Manuscript Author Manuscript Author Manuscript

decrease prior to episode onset. The linear descent in NE suggests complete silence of LC activity during and prior to REM sleep, which is also apparent from the lack of LC activity. Furthermore, we show that low NE is a requirement of REM sleep induction. The necessity of low LC/NE activity for REM sleep induction is supported by several studies[49,50] likely through the permissive effect of low NE on activation of the pedunculopontine nuclei[51], though controversies exist[15,20].

Both sleep spindles and REM sleep are implicated in memory consolidation processes[1,2,52,53]. If pronounced NE descents are associated with higher spindle incidents during IS-REM sleep transitions, larger NE oscillatory amplitudes may be particularly important for memory performance. In order to increase NE oscillatory amplitude, we optogenetically silenced the LC during sleep at regular intervals. This intervention led to build-up of spindle activity and induced sleep sequences resembling IS and REM sleep (Figure 3). Remarkably, we could enhance memory performance; a strong correlation between the induced spindle activity and subsequent memory performance for the individual animals was evident when LC was silenced. It has been hypothesized that the sequential order of IS and REM sleep serves an important function, where memory representations tagged by spindles are further processed during REM sleep[54,55]. Neither duration nor frequency of REM sleep correlated with individual behavioral performances, indicating that spindle-rich IS sleep might be a better marker for memory performance. In support of these findings, pharmacological and optogenetic elevation of NE abolishing NE oscillations resulted in expression of spindle-poor NREM sleep, elimination of IS to REM sleep transitions and compromised memory performance. These findings support previous studies demonstrating that optogenetic or electrical activation of LC during sleep disrupts spindle generation and reduces memory performance[22,25], which we ascribe to abolishment of NE oscillations. While NE reuptake inhibition has been demonstrated to reduce spindle-dependent memory[36], other studies show that this treatment increases memory performance[56,57]. However, the latter studies did not show upregulation of NE levels, which may explain the discrepancies. Furthermore, the effects on sleep of systemic elevation of NE is complex as it can involve multiple neuromodulator systems and receptor targeting[34,35]. Our results pinpoint the need for future therapeutic strategies focusing on maintaining NE oscillation amplitude and intact sleep microarchitecture. The data presented here suggest that treatment focusing on enhancing NE oscillations might provide a powerful therapeutic tool in promoting the memory-enhancing segments of sleep.

While it is unlikely that awakening directly benefit memory consolidation, we observed that increased awakenings is an integral part of higher NE oscillation amplitude and IS-REM sleep sequences. Thus, our observations may suggest that the full consolidation potential of normal sleep is not exploited due to the prevalence of infraslow NE oscillations keeping its amplitude to a level that upholds mainly NREM sleep in exchange for IS-REM sleep sequences and awakenings. Furthermore, our observations may explain why excessive micro-arousals have previously been associated with performance reductions[5-7]. We show that gradually increasing the number of micro-arousals through NE threshold-based LC optogenetic activation reduces the oscillatory amplitude of NE needed for spindle build-up in a titrated manner that leads to an overall reduction in spindles and memory consolidation (Figure 4). An interesting consideration is that micro-arousals and awakenings are by

Author Manuscript Author Manuscript Author Manuscript Author Manuscript

nature sleep-fragmenting events, which are in general considered detrimental to memory performance. However, our results suggest that this interpretation should be revisited and that the impact on memory consolidation depends on the sleep micro-architecture associated with the sleep fragmentation. Thus, awakenings are more strongly linked to IS-REM sleep transitions than micro-arousals.

If low NE levels are a prerequisite for spindle induction and memory performance, why are intrinsic LC-NE-driven micro-arousals such an inherent part of sleep? It is tempting to speculate that NE oscillations may serve to sustain NREM sleep through cyclic interruptions of NE descents that would otherwise lead to IS-REM sleep induction. So, what governs whether an LC activation during sleep results in a micro-arousal versus an awakening? The experimental design of this study allowed us for the first time to define how the cyclic changes in NE levels predict whether phasic LC activation results in micro-arousals or an awakening. One of the most surprising observations was that prolonged periods of natural NE descent (~40-50 s) increased the likelihood of awakening in response to both intrinsic and external arousal input. Further, we find that REM sleep associated with longer periods of LC silence compared to NREM sleep more often result in awakenings when LC is re-activated, leading to the important notion that the relative increase in NE is a better predictor of awakening than absolute NE level. Thus, shifting NE amplitudes heavily influences the ability to mediate brain state transitions. Several studies have demonstrated that the α2-adrenergic receptor inhibits LC cell firing and blockade of this receptor increases the excitability of LC neurons[58,59]. Thus, long durations of NE descent likely reduce α2-mediated inhibition and facilitates the excitability of LC neurons, which increases the propensity towards arousal.. Similarly, Hayat et al.[60] demonstrates enhanced sound-triggered awakening during REM sleep. It is conceivable that the 30 s periodicity of LC activation during NREM sleep reflects a feedback mechanism that limits the extent of NE descent thereby keeping LC auto-inhibition to a level that reduces the risk of awakenings and promotes micro-arousals. Hayat et al. also discovered that higher levels of tonic LC activity in sleeping rats increases sensitivity towards external stimuli[60]. A plausible explanation is that lowering of α2-mediated inhibition of LC neurons leads to membrane depolarization and reduced spiking threshold resulting in dispersed tonic LC firing. While it is not clear how this elevation in tonic firing of LC neurons contributes to cortical NE level, a recent study shows that condensed phasic-like LC-NE axonal activity more effectively releases NE in the cortex[61].

In this study, we demonstrate that infraslow NE oscillations are a key player in shaping sleep microarchitecture. Specifically, tuning down NE oscillatory amplitude favors micro-arousals thus sustaining NREM sleep, while promoting NE descent boosts spindle occurrences associated with IS sleep, but primes awakenings. It is possible that prior reports documenting compromised cognitive performance due to disturbed sleep with frequent interruptions[38] could be explained by a reduction in the oscillatory amplitude of NE, which reduces the restorative aspects of sleep, while increasing the number of micro-arousals.

Author Manuscript Author Manuscript Author Manuscript Author Manuscript

Methods

Mice

Wildtype C57BL/6 mice were acquired from Janvier Labs at 7 weeks of age. Heterozygous TH::Cre mice were bred on a C57BL/6 background. Both male and female mice were used. Animals were housed with unlimited access to food and water in a normal 12-h light/dark cycle at 21°C with 40-60% humidity. Animals were 12-20 weeks old at time of behavioral assessment. All experiments were approved by the Danish Animal Experiments Inspectorate and were overseen by the University of Copenhagen Institutional Animal Care and Use Committee (IACUC), in compliance with the European Communities Council Directive of 22 September 2010 (2010/63/EU) legislation governing the protection of animals used for scientific purposes.

Surgery

All surgeries were performed in accordance with institutional guidelines. Mice were 7-15 weeks old at time of surgery. General anesthesia was induced using 5% isoflurane, and maintained at 1-3% isoflurane. The mice were placed in a stereotactic frame and received preoperative buprenorphine (0.05 mg/kg) for general analgesia along with lidocaine (0.03 mg/kg) at the incision site. An incision was made on the scalp between the ears and the skull was aligned. Four burr holes were drilled in the skull with an electrical drill (Tech2000, RAM Microtorque) according to stereotactic coordinates relative to bregma. In mPFC, we injected AAV9-hSyn-GRAB$_{NE2m}$ under the neuronal hSyn promoter (provided by Yulong Li). Simultaneously, we injected AAV5 encoding floxed GCaMP6f in LC in a TH-Cre driver mouse line. Stereotactic coordinates used for mPFC injections: A/P +1.7 mm, M/L −0.3 mm, and D/V −2.00, −2.25, −2.50, and −2.75 mm (125 nL virus infused at each depth) and for LC injections: A/P −5.5 mm, M/L: −0.9 mm, and D/V: −3.2 mm, −3.4 mm, - 3.6 mm, and −3.8 mm (125 nL at each depth). Virus was infused at 100 nL/min and the needle was left in place for additional 7 minutes and then slowly withdrawn. 0.8 mm low impedance stainless steel screws (NeuroTek) were screwed into two burr holes located above frontal cortex (contralateral side from the optic implant), and above the cerebellum (reference area). Two silver wires (W3 Wires International) were inserted into the trapezius muscle serving as an EMG electrode. Mono fiber-optic cannulas (400 μm,0.48 NA, Doric Lenses) attached to a 2.5 mm diameter metal ferrule were then implanted in mPFC (A/P 1.7 mm, M/L −0.3 mm, D/V −2.50) and LC (A/P −5.5 mm, M/L: −0.9 mm, D/V: −3.65 mm) and cannulas and screws were fixed to the skull using dental cement (SuperBond). Prior to waking up, animals received carprofen (5 mg/kg) s.c.. A minimum of two weeks were allowed for sufficient expression and recovery.

For optogenetic LC experiments, AAV5/2 encoding floxed ArchT-eGFP or floxed hChR2-eYFP were injected bilaterally in LC at A/P −5.5 mm, M/L: +/−0.9 mm, D/V: −3.75 mm (300 nL virus) and dual fiber-optic cannula (200 μm, 0.22 NA, Doric Lenses) were implanted above LC (D/V: −3.65 mm).

Author Manuscript Author Manuscript Author Manuscript Author Manuscript

Construct	Company/provider	Cat#
pAAV9-hSyn-GRAB$_{NE2m}$	Yulong Li lab	
AAV5-Syn-FLEX-GCaMP6f-WPRE-SV40	Addgene	100833-AAV5
pAAV-hSyn-GRAB_NEmut	Addgene	123310-AAVrg
ssAAV5/2-shortCAG-dlox-ArchT-eGFP-dlox-WPRE-SV40p(A)	Zürich vector Core	V461-5
ssAAV5/2-hEF1a-dlox-hChR2(H134R)-eYFP(rev)-dlox-WPRE-hGHp(A)	Zürich vector Core	v214-5
AAV5-EF1a-DIO-EYFP	UNC Vector Core	
pAAV9-hSyn-GRAB$_{DA1h}$	Addgene	113050-AAV9

Fiber photometry

Two pairs of excitation LEDs (465 nm and 405 nm, Doric Lenses, Tucker Davis Technologies) were connected to each their minicube (Doric Lenses) by attenuator patch cords (400-μm core, NA = 0.48, Doric Lenses). The minicube optics allow for monitoring of fluorophores using dichroic mirrors and cleanup filters chosen to match the excitation and emission spectra. LEDs were controlled by LED drivers (Thorlabs, Doric, Tucker Davis Technologies) and connected to a RZ-5 or RZ10-X real-time processor (Tucker-Davis Technologies). In mPFC, 465 nm and 405 nm excitation light were delivered through the same patch cord to excite GRAB$_{NE2m}$ fluorescence, while 405 nm was an excitation isosbestic wavelength for GCaMP6f correcting for bleaching and signal fluctuations due to movement. In LC, using the same patch cord, excitation light at 465 nm was used to stimulate GCaMP6f fluorescence and 405 nm added as control. 465 nm/405 nm excitation were sinusoidally modulated at 531 Hz/211 Hz. Fiber-optic patch cords (400 μm core, NA = 0.48, Doric Lenses) provided a light path between the minicubes and the animals. Zirconia sleeves were used to attach fiber-optic patch cords to fiber implants on the animal.

Each of the four modulated signals generated by the four LEDs were independently recovered using standard synchronous demodulation techniques implemented on the RZ-5/RZ10-X real-time processor (sampling rate of 1000 Hz). The Synapse software (Tucker-Davis Technologies) was used to control the signal processor and align fluorescent signals with video and EEG/EMG signals through in- or out-coming TTL pulses. Files were exported for analysis to MATLAB R2020a (MathWorks). ΔF/F calculations were based on the fitted 405 nm signal or by using the median of the fluorescence signal itself. For 405 fitting, first, the scale of the 465 nm signal and isosbestic 405 channel was normalized by using a least-squares (MATLAB *polyfit* function) to determine the slope and intercept needed in order to generate a scaled 405 nm channel:

$$scaled\ 405\ nm\ channel = a * 405\ nm\ channel + b$$

Next, ΔF/F is generated by subtracting the fitted control channel from the signal channel:

$$\Delta F\ /\ F\ (\%) = (signal\ 465\ nm - scaled\ 405\ channel) * 100\ /\ scaled\ 405\ channel$$

Author Manuscript Author Manuscript Author Manuscript Author Manuscript

In order to characterize NE oscillations across all NREM and REM sleep phases, we calculated NE peak level (90% percentile) and NE trough level (10% percentile) across NREM or REM sleep phases, respectively, during 3 hours of sleep recordings. NE amplitude was calculated by subtracting NE trough values from NE peak values. The oscillation frequency of NE was calculated by selecting NE peaks throughout NREM sleep across 3 hours of sleep recordings (MATLAB *findpeaks* function, minimum inter-trial interval of 10 s, minimum amplitude of 1.5 ΔF/F (%) and diving it by the total duration of NREM sleep. Multitaper power spectral analysis was done on NE traces across NREM sleep, REM sleep and wake to assess low-frequency oscillatory patterns (MATLAB *pmtm* function).

To characterize NE signal across MA^{NE}, $MA^{EEG/EMG}$ and $wake^{EEG/EMG}$ transitions, NE signal was aligned according to the minimum NE trough level immediately proceeding the transition and summarized NE trough levels was calculated by taking the 10% percentile from −10 to 0 s and NE peak level (90^{th} percentile) from 0 to 50 s. The NE ascend amplitude was defined as the difference between NE peak and trough. NE descend time and slope was calculated by finding the onset of maximal NE peak proceeding the descend, and calculating the distance between this point and the minimal NE trough value. Slope of the NE signal between these values was calculated by a linear regression fit. With optogenetic suppression of LC, the NE descent amplitude induced by laser onset was calculated by subtracting the 5% percentile from 90 s post onset from the mean value 60 s pre onset, while the NE ascent amplitude at laser offset was calculated by subtracting 95% percentile 90 s post offset from the mean value 60 s pre offset.

Sleep measurements

Mice were placed in recording chambers (ViewPoint Behavior Technology) and cables were connected to the EEG and EMG electrodes. Cables were connected to a commutator (Plastics One, Bilaney, SL12C) and the mice were allowed to habituate to the recording chamber (ViewPoint Behavior Technology) for at least one day prior to recordings. On the day of recording, mice were connected to fiber optic implants and recordings were done for 2-4 h during their light phase. EEG and EMG signals were amplified (National Instruments Inc., 16-channel AC amplifier Model 3500) and filtered (EEG signal: high-pass at 1 Hz and low-pass at 100 Hz; EMG signal: high-pass at 10 Hz and low-pass at 100 Hz), and a notch filter of 50 Hz was used to reduce power line noise. Signals were digitized using a Multifunction I/O DAQ Device (National Instrument, USB-6343) and sampled at a sampling rate of 512 Hz. Video was recorded continuously using an infrared camera (Flir Systems) and used later to aid in the scoring of vigilance states. Hypnograms were created by visual inspection of EEG traces divided into 5 and subsequently 1 s epochs. Vigilance states were defined as wake (high muscle tonus and a high frequency, low amplitude EEG), NREM sleep (no muscle tonus and low frequency, high amplitude EEG,), and REM sleep (no muscle tonus and high frequency, low amplitude EEG). We categorized wake bouts of < 15 s as micro-arousals (Figure 1b). In addition, we defined local EEG changes (combined theta, sigma and beta power reductions, Extended Data Figure 1) without EMG changes during NREM sleep as MA^{NE}. Analysis of hypnograms was done using SleepScore software (ViewPoint Behavior Technology). All data analysis was subsequently performed in MATLAB using custom-made scripts. The power spectral densities at frequencies 1-30

Author Manuscript Author Manuscript Author Manuscript Author Manuscript

Hz were calculated using Welch's method with a 5 sec Hamming window and the logarithm of the power was calculated for each frequency. The average power for different frequency bands was determined (delta: 1-4; theta: 4-8; sigma: 8-15; beta: 15-30). In order to detect spindles, collected LFP signal in the S1 cortex (n = 4) was bandpass filtered in the 8-15 frequency range and subsequently squared. A threshold of 0.8 times the standard deviation above the mean value was applied and peaks crossing this threshold smoothed trace and lasting >0.5-10 s was marked as putative spindles. Events separated by < 20 ms were merged as a single event. In all sleep recordings without interventions (Figure 1 and Figure 2), two mice were excluded from sub-panels relating to LC Ca^{2+} measurements due to mistargeting of virus injection, and one mouse from REM sleep analysis (due to no REM sleep episodes>150 s).

Cross-correlation analysis between continuous functions of NE levels and sigma or delta power traces was done across 10 min NREM sleep periods. Specifically, NE recordings were down-sampled 100 times and corresponding sigma or delta power calculations were up-sampled to match the NE recordings.

In a subset of sleep recordings animals (n = 7) were administered desipramine (10 mg/kg, 10 mL/kg) by i.p. injection and left to record for 3.5 hours. On another day (minimum 3 days apart from the desipramine injection), the same animals underwent similar recordings where they received a saline injection (10 mL/kg) to get within-animal controls. Analysis was done on 1-3.5 h period after administration due to difficulties classifying sleep based on EEG patterns during the first hour after administration

Auditory stimulation

During sleep recordings as described above, a new batch of mice (n = 6) were subjected to auditory stimulations (0.5 s, 80 dB) at a 4 min interval. Subsequently sounds during NREM sleep were selected and divided into outcome (sleep/arousal) based on the reduction in the sigma power (> 0.1 $\log(\mu V^2)$ within 5 s following the sound.

Optogenetic inhibition of LC

A 532 nm laser (Changchun New Industries Optoelectronics Tech. CO., Ltd., model: 16030476) was used to generate 2 min stimulations (5 mW at the tip of the fiber) bilaterally in LC simultaneously with mPFC fiber photometry recordings and EEG and EMG measurements. Mice were left undisturbed in EEG recording chambers during the light phase allowing for natural sleep/wake behavior, while being recorded on infrared camera. Animals were simulated every 10 min regardless of vigilance state. Stimulations initiated during NREM sleep were subsequently selected for analysis. n = 9 Arch, 5 YFP; however, one Arch mouse was excluded from subpanels relating to NE measurements due to low $GRAB_{NE2m}$ expression (n = 8) and one YFP mouse was excluded from subpanels relating to sigma power due to noisy EEG signal (n = 4).

Optogenetic activation of LC

A 430-490 nm laser (Shanghai Laser & Optics Century Co., Ltd., model: BL473-200FC) was used to generate 2 s stimulations of 10 ms pulses at 20 Hz (5 mW at each fiber tip)

Author Manuscript Author Manuscript Author Manuscript Author Manuscript

bilaterally in LC simultaneously with $GRAB_{NE2m}$ recordings from mPFC. 2 h of baseline recordings without laser stimulation was followed by 5 hours of closed-loop stimulation where threshold crossing of smoothed real-time calculation of ΔF/F (%) calculations of NE levels based on 2 min windows (Synapse, Tucker Davis Technologies) elicited laser stimulations. Thresholds were set at −15 ΔF/F (%) and increased in increments of 5 ΔF/F (%) once per hour until +5 ΔF/F (%). After the 5 hours of laser stimulations, recording continued for another 2 h without laser stimulations. All output measurements from laser manipulation (fig. 4d and f-j) are normalised within animal to the baseline value prior to first laser stimulation period. n = 7 ChR2, 7 YFP; however, one YFP mouse was excluded in subpanels relating to sigma power due to noisy EEG signal (n = 6).

Novel object recognition

Animals were habituated to an open field for 10 min followed by a resting period in their home cage for 5 min while two identical objects were placed in the open field. The animals were then habituated to the objects for 15 min, followed by desipramine administration (10 mg/kg, 10 mL/kg, n = 7) or saline (10 mL/kg, n = 9) and allowed to sleep for 3 hours. A novel object replaced one of the familiar objects, and the animals were allowed to explore the two objects for 5 min. A separate group of animals expressing Arch (n = 9) in LC for optogenetic suppression or YFP (n = 5), were habituated to initial objects for 10 min, followed by two hours in the EEG recording chamber, where we recorded EEG, EMG and $GRAB_{NE2m}$ fluorescence while the animals were optogenetically stimulated as described above, but with 2 min stimulations every 6 min before 5 min of novel object exposure. In another group of animals expressing either ChR2 (n = 7) or YFP (n = 7) in LC for optogenetic activation, animals were familiarized with two objects for 15 min to ensure that YFP control could remember the objects. Animals were then allowed to sleep for 2 hours while being optogenetically stimulated with a $GRAB_{NE2m}$ threshold=0 as described above before 5 min of novel object exposure. This was all done during the light phase to encourage natural sleep between the encoding and recall phase. Ethovision XT 11.5 (Noldus) was used to track videos of the behavioral tasks.

Immunohistochemistry

To validate location of optic implant and virus expression, we did immunostaining on brain sections. Animals were deeply anesthetized using ketamine/xylazine, then perfused with PBS followed by 4% PFA. Brains were dissected and post-fixed in 4% PFA overnight and transferred to PBS until sectioning. 60 μm sections surrounding the implants were cut using a vibratome. Sections were then blocked in PBS with 5% goat serum and 0.3% Triton X-100 at room temperature for 1-2 h before overnight incubation with primary antibodies at 4° C. After washing, sections were incubated with secondary antibodies at room temperature for 2 h, then incubated with DAPI for 2-10 min.

Images of whole brain slices were acquired using a Nikon Instruments Ni-E motorized microscope equipped with a 4x CFI Plan Apo Lambda objective (0.2 NA). For excitation, halogen light source was used in combination with excitation filters 362-389 nm, 465-495 nm, 530-575 nm, and Cy5 628-640 nm. 4x4 images were acquired per section and stitched together automatically using NIS Elements AR software from Nikon. Close-up images were

Author Manuscript Author Manuscript Author Manuscript Author Manuscript

acquired using a Nikon Instruments C2+ Ti-E Confocal laser-scanning microscope with a 20x CFI Plan Fluor MI objective (0.75 NA) or a 40x CFI Plan Fluor oil objective (1.30 NA). The excitation sources were 405 nm, 561 nm, and 640 nm laser diodes and a 488 nm solid-state diode laser. For the 40x images we acquired Z-stacks ranging from 20-40 μm and flattened them in Fiji/ImageJ using standard deviation of intensity.

Primary antibodies

Name	Company/provider	Cat#
anti-RFP antibody, 1:500	Abcam	ab62341
Anti-GFP (Green Fluorescent Protein) (Chicken Antibodies, IgY Fraction), 1:500	Aves	GFP-1020
GFP Polyclonal Antibody 1:500	Thermo Fisher Scientific	A-6455
Mouse Anti-Neuronal Nuclei (NeuN) Monoclonal Antibody, clone A60, 1:100	Merck Millipore	MAB377
Anti-Tyrosine Hydroxylase, clone LNC1, 1:500	Merck Millipore	MAB318

Secondary antibodies

Name	Company/provider	Cat#
Goat anti-Rabbit IgG (H+L) Highly Cross-Adsorbed Secondary Antibody, Alexa Fluor 488	Thermo Fisher Scientific	A11034
Goat anti-Chicken IgY (H+L) Secondary Antibody, Alexa Fluor 488	Thermo Fisher Scientific	A11039
Goat anti-Rabbit IgG (H+L) Cross-Adsorbed Secondary Antibody, Alexa Fluor 568	Thermo Fisher Scientific	A11011
Goat anti-Chicken IgY (H+L) Secondary Antibody, Alexa Fluor 568	Thermo Fisher Scientific	A11041
Goat anti-Mouse IgG1 Cross-Adsorbed Secondary Antibody, Alexa Fluor 647	Thermo Fisher Scientific	A21240

High-Performance Liquid Chromatography

Tissue samples (n = 11) were immediately frozen on dry ice and stored at −80°C until homogenized in 250 μl perchloric acid 0.1 N. Following centrifugation at 14,000 × *g* for 30 min, 200 μl of the supernatant was filtered through a glass 0.22-μm filter (Avantec 13CP020AS). The samples were analyzed using EC-HPLC methodology. The concentrations of monoamines and metabolites were determined by HPLC with electrochemical detection. The column was a Prodigy 3 μm ODS-3 C18 (DA 2 × 100 mm, particle size 3 μm, Phenomenex, YMC Europe). The mobile phase (55 mM sodium acetate, 1 mM octanesulfonic acid, 0.1 mM Na_2EDTA, and 8% acetonitrile, pH 3.2) was degassed with an online degasser. Samples (10 μl) were injected with a flow rate of 0.15 ml/min. The electrochemical detection was accomplished using an amperometric detector (Antec Decade) with a glassy carbon electrode set at 0.8 V and an Ag/AgCl reference electrode. The output was recorded and peak areas were calculated by LC solution software (Shimadzu).

Author Manuscript Author Manuscript Author Manuscript Author Manuscript

Foot shock with $GRAB_{DA1h}$ sensor

Fiber photometry measurements were obtained from mice (n = 5) expressing the dopamine sensor, $GRAB_{DA1h}$, in mPFC (surgery as described above) during a foot shock paradigm with pharmacological blocking of dopamine reuptake. The mice were habituated to a foot shock chamber for 5 min before receiving foot shocks (0.45 mA, 0.5 s) every 3 minutes until a total of 11 foot shocks. After the third foot shock, mice received a dose of GBR 12909 hydrochloride (Tocris, Cat# 0421) via an i.p. injection (10 mg/kg, 10 mL/kg) or saline (10 mL/kg).

Statistics and Reproducibility

No statistical methods were used to pre-determine sample sizes but our sample sizes are similar to those reported in previous publications[15,22]. Manipulations were counter-balanced and randomized across mice. The majority of data collection and analysis were not performed blind to the conditions due to the automatic nature of the experiments and analysis. The Shapiro-Wilk test was used to assess normality of data. Two-sided paired t-test or unpaired t-test was employed to compare pairs of groups, if data passed the normality test. Otherwise, the Wilcoxon matched-pairs signed rank test or Mann-Whitney test was used for comparison. One sample t-test was used to test whether population mean was different from a specific value. For repeated measurements, one-way or two-way ANOVAs with Šídák's hoc test were used, respectively.

Immunohistochemical experiments were repeated independently with similar results in up to three animals.

Extended Data

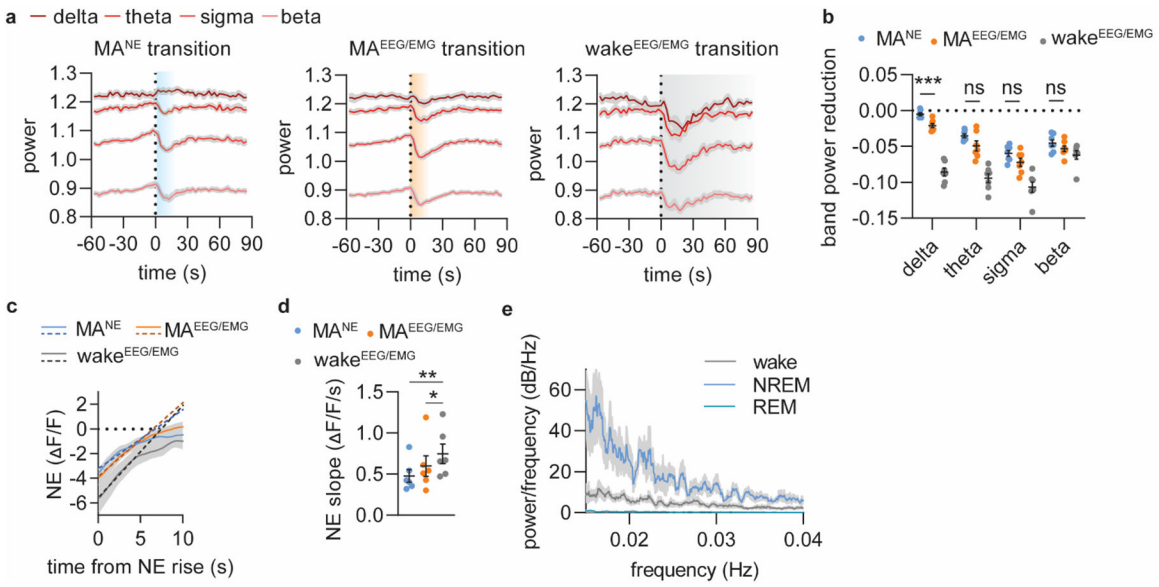

Extended Figure 1. All ascending stages of NE oscillations are associated with EEG-defined micro-arousals or awakenings.

Author Manuscript Author Manuscript Author Manuscript Author Manuscript

a. Mean power traces for delta, theta, sigma and beta frequency bands aligned to NE rise associated with EEG/EMG-based transitions from NREM sleep to continued NREM sleep (blue, MA^{NE}), micro-arousals ($MA^{EEG/EMG}$, orange) and wake (grey, $wake^{EEG/EMG}$). **b**. Summary plot showing the reduction in band power across the different transitions. There was no difference between MA^{NE} and $MA^{EEG/EMG}$ for theta, sigma and beta band power, which are the frequencies used to assess micro-arousals. Significance was calculated by means of two-way repeated measures ANOVA with Šídák's post hoc test (only MA^{NE} and $MA^{EEG/EMG}$ post hoc comparisons shown in graph for simplicity, $P = 0.0003$, delta; $P = 0.13$, theta; $P = 0.11$, sigma; $P = 0.65$, beta). **c.** Slope of linear regression on 5 initial seconds of NE rise was used as estimate for rise time. **d.** NE slope across the different type of transitions (repeated measures one-way ANOVA with Tukey's multiple comparisons test, $P = 0.0059$, MA^{NE} vs wake; $P = 0.041$, $MA^{EEG/EMG}$ vs wake). **e.** Multi-taper power spectral analysis showed increased power for slower frequencies for NREM sleep compared to wake and REM sleep with no defined peak frequency likely due to the discrete nature of NE oscillations. n = 7. Data is shown as mean±SEM. ***p < 0.001.

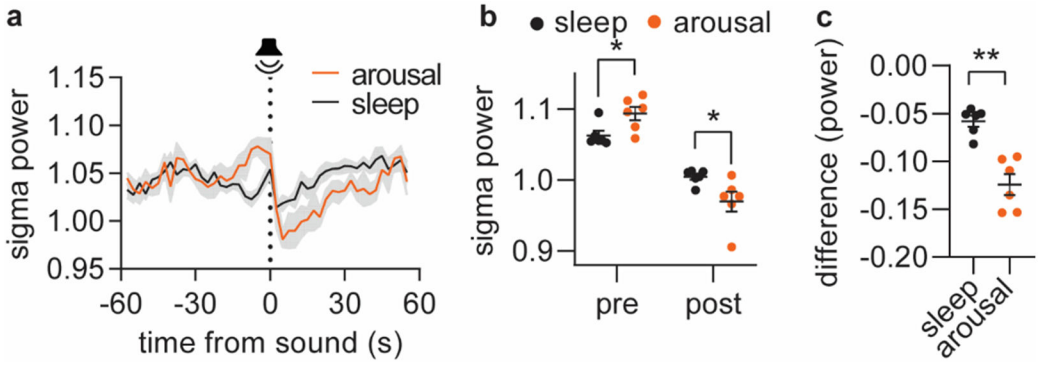

Extended Figure 2. Decrease in sigma power marks tone-evoked arousal.

Based on the local decline in sigma power in response to tone (> 0.1 log(μV^2)), the tone outcome was divided into arousal and otherwise maintained sleep. **a.** Mean sigma power traces in response to tone leading to either arousal or persistent sleep. **b.** The maximum value of sigma power maximum prior to tone ('pre') and the minimum sigma power after the tone ('post') for the defined arousal and sleep conditions. **c.** The difference in sigma power occurring in response to the tone. Significance was calculated by means of two-way repeated measures ANOVA with Šídák's post hoc test (**b**, $P = 0.035$, pre; $P = 0.023$, post) or two-tailed paired *t*-test (**c**, $P = 0.0034$). n = 6. Data is shown as mean±SEM. *p < 0.05, **p < 0.01.

Author Manuscript Author Manuscript Author Manuscript Author Manuscript

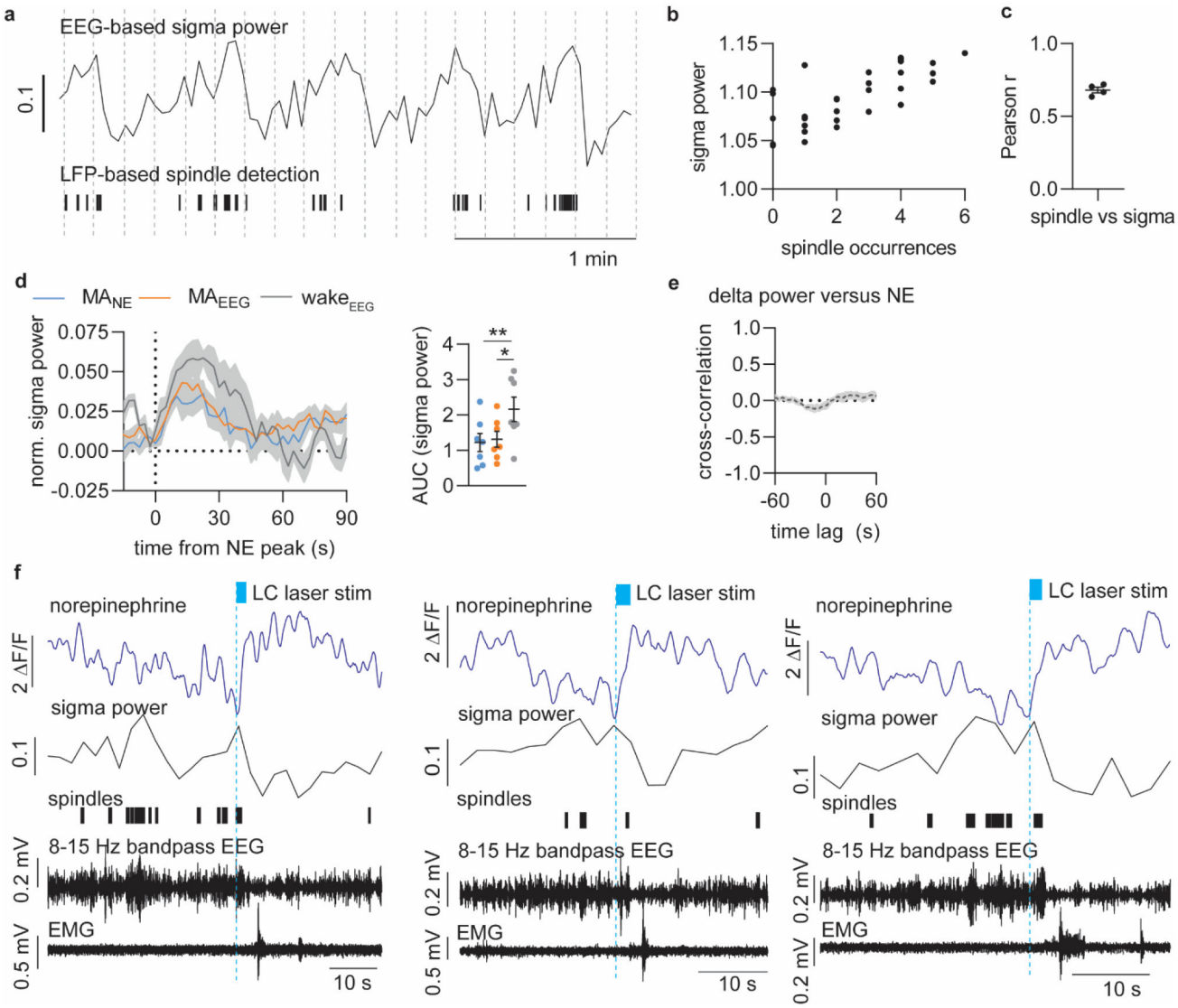

Extended Figure 3. Supplementary Figure S6. Relationship between norepinephrine, sigma power, spindles and delta power.

a. Representative trace showing sigma power of surface EEG recordings with corresponding detection of spindles based on S1 cortical LFP recordings. **b.** Correlation between spindle occurrences and mean sigma power across 10 s bins over a 5 min NREM sleep episode. **c.** Mean Pearson r values (0.63 +/− 0.02). **d.** Mean sigma power traces normalized to baseline showing the amount of sigma power increase associated with NE descents preceeding microarousals (MA_{NE} or $MA_{EEG/EMG}$) or awakenings ($wake_{EEG/EMG}$). Calculated area under the curve (AUC) for sigma power is largest during the NE descents associated with awakenings transitions (two-tailed paired *t*-test; $P = 0.60$, MA^{NE} vs $MA^{EEG/EMG}$; $P = 0.0057$, MA^{NE} vs wake; $P = 0.044$, $MA^{EEG/EMG}$ vs wake).**e.** Mean correlation coefficient between delta power and NE level (5 min NREM sleep episodes) **f.** Three different example traces showing how optogenetic activation of locus coeruleus (LC, 2 s 20 Hz 10 ms pulses) during periods of NE descend leads to NE ascend followed by a delayed change in spindle occurrences and amplitude reduction of 7-15 bandpass filtered EEG that is not represented

by sigma power (window = 5 s, overlap: 2.5 s). n = 4 (**c**); n = 7 (**d-e**). Data is shown as mean±SEM. *p < 0.05, **p < 0.01.

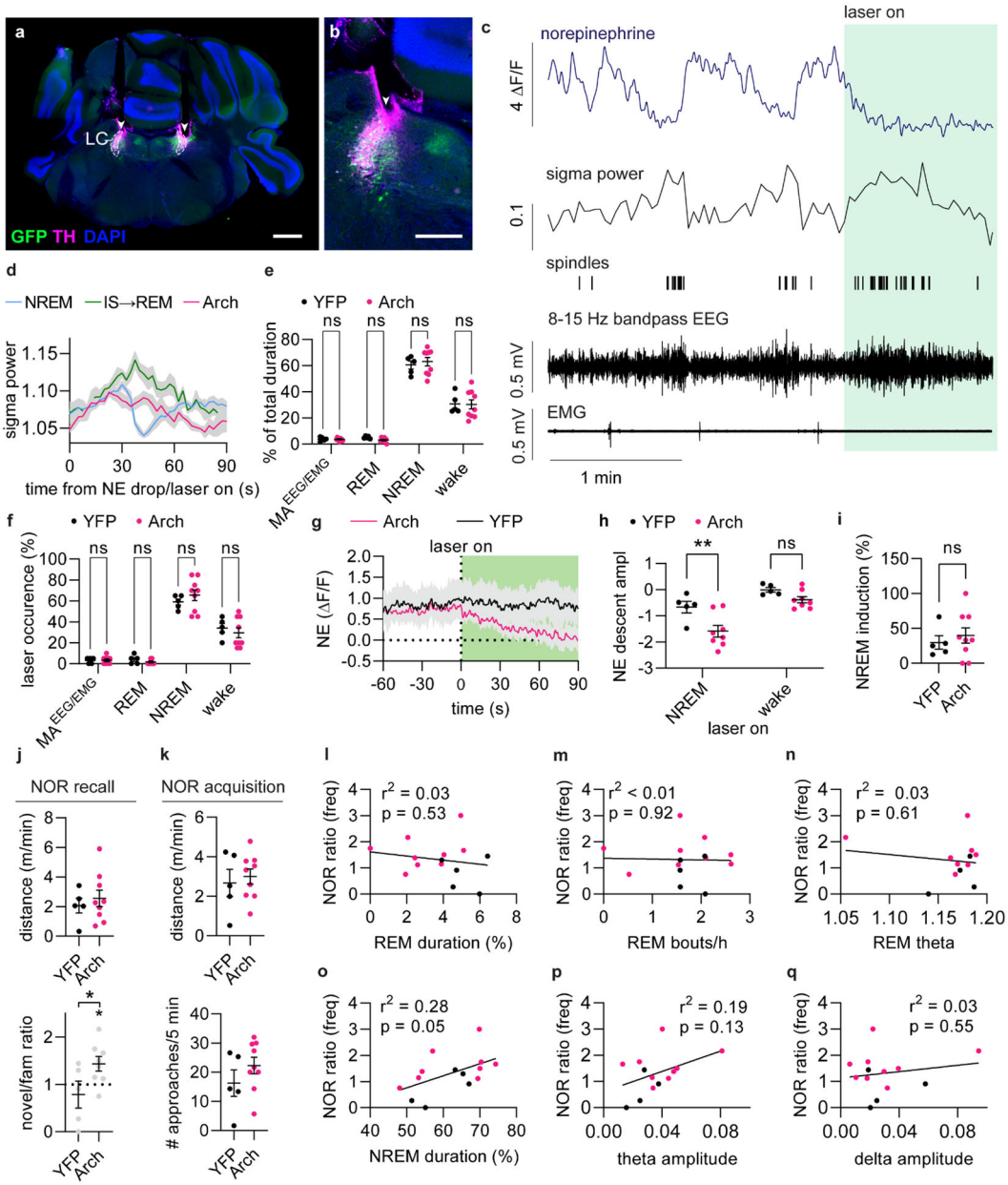

Extended Figure 4. Optogenetic suppression of LC.

a. Arch expression in LC was verified by co-staining for TH and GFP. Arrowheads indicate the tip location of the optic fiber (scale bar = 800 μm). **b.** Close up of **a** (scale bar = 400 μm). **c.** Example traces showing norepinephrine level, sigma power, sleep spindles, bandpass LFP in sigma range, and EMG raw data. **d.** Mean sigma power aligned to onset of NE drop (NREM and IS-REM) or onset of laser stimulation (Arch). **e.** Time spent in sleep/wake stages during 2 h recording between memory encoding and recall (2-way repeated measures ANOVA with Šídák's multiple comparison post hoc test). **f.** Number of laser stimulation (%

Author Manuscript Author Manuscript Author Manuscript Author Manuscript

Author Manuscript Author Manuscript Author Manuscript Author Manuscript

of total number) in each sleep/wake stage (2-way repeated measures ANOVA with Šídák's multiple comparison post hoc test). **g.** Mean NE trace at laser onset during wakefulness. **h.** NE descent amplitude induced by laser onset during NREM and wakefulness (2-way repeated measures ANOVA with Šídák's multiple comparison post hoc test, $P = 0.0046$, NRREM). **i.** Percentage of laser stimulations during wakefulness resulting in transition to NREM sleep (unpaired *t*-test). **j.** Distance moved and ratio between approaches during the recall phase of the novel object recognition (NOR) (two-tailed unpaired *t*-test, $P = 0.049$, one-sample *t*-test $P = 0.49$, YFP; $P = 0.026$, Arch). **k.** Distance moved and object approaches during the acquisition phase of the NOR (unpaired *t*-test). **l.** Linear regression between object exploration ratio and time spent in REM sleep. **m.** Linear regression between object exploration ratio and number of REM bouts/h. **n.** Linear regression between object exploration ratio and mean theta power during REM sleep. **o.** Linear regression between object exploration ratio and time spent in NREM sleep. **p.** Linear regression between object exploration ratio and theta amplitude in response to laser. **q.** Linear regression between object exploration ratio and delta amplitude in response to laser. n = 9 Arch, 5 YFP. Data is shown as mean±SEM. *p < 0.05, **p < 0.01.

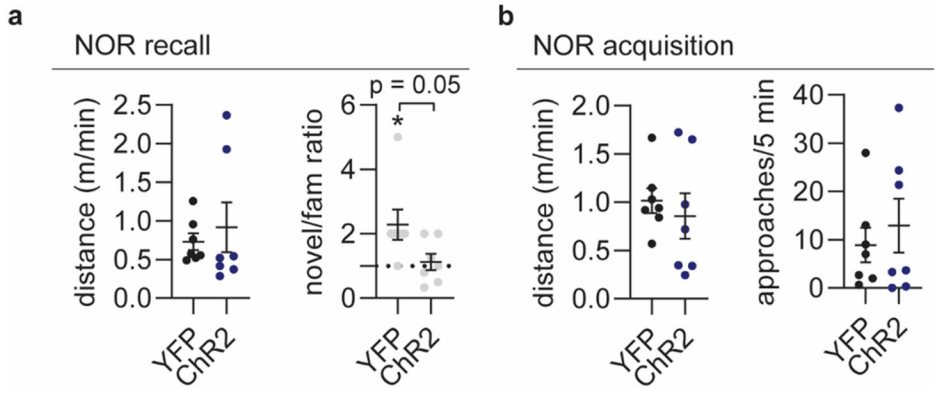

Extended Figure 5. Optogenetic activation of LC.

a. Distance moved and ratio between novel and familiar object approaches during recall phase of novel object recognition (two-tailed unpaired t test, $P = 0.052$, one-sample t test, $P = 0.35$, YFP; $P = 0.64$, ChR2). **b.** Distance moved and object exploration during memory acquisition (right) (unpaired t test). n = 7 ChR2, 7 YFP. Data is shown as mean±SEM. *p < 0.05.

Author Manuscript Author Manuscript Author Manuscript Author Manuscript

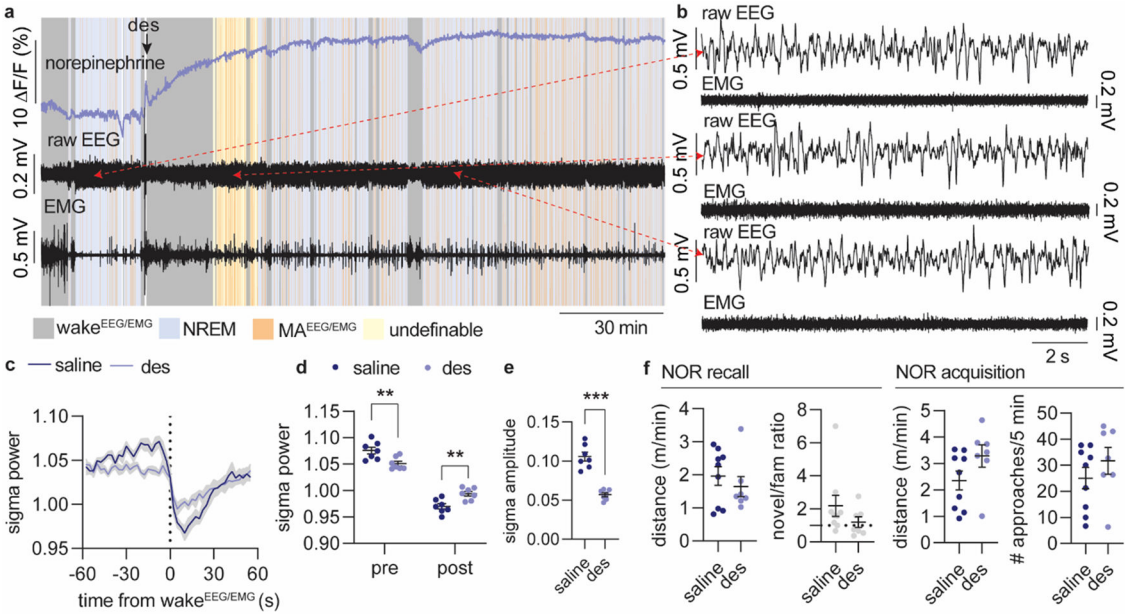

Extended Figure 6. The effect of NE reuptake inhibition on EEG and arousability.

a. Representative traces of norepinephrine, raw EEG and EMG before and after administration of the NE reuptake inhibitor, desipramine (des, 10 mg/kg). **b.** Example EEG and EMG traces from NREM sleep prior to desipramine administration (top), during undefinable phases following desipramine administration (middle) and from defined NREM sleep following administration with desipramine (bottom). **c.** Sigma power traces aligned to the onset of awakenings (wake$^{EEG/EMG}$) following either treatment with saline or desipramine. **d.** Mean sigma power before and after NREM-wake$^{EEG/EMG}$ transition (2-way repeated measures ANOVA with Šídák's multiple comparison post hoc test, $P = 0.0024$, pre; $P = 0.031$, post). **e.** Reduction in sigma power amplitude (two-tailed paired t-test, $P = 0.0007$). **f.** Distance moved and ratio between novel and familiar object approaches during the recall phase of the novel object recognition (NOR) as well as distance moved and number of object approaches during the acquisition phase (unpaired t-test and one-sample t-test). n = 7 (**c**-**e**), n = 7 des, 9 sal (**f**). Data is shown as mean±SEM. **p < 0.01, ***p < 0.001.

Supplementary Material

Refer to Web version on PubMed Central for supplementary material.

Acknowledgements

Funding:

Lundbeck Foundation, R386-2021-165, MN

Independent Research Council Denmark, 7016-00324A, MN and CK

Augustinus Foundation, 16-3735, CK

Novo Nordisk Foundation, NNF20OC0066419, MN

Author Manuscript Author Manuscript Author Manuscript Author Manuscript

U.S. Department of Health & Human Services, NIH, R01AT011439, MN

Department of Defense, Army Research Office, W911NF1910280, MN

The Simons Foundation, 811237, MN

National Key R&D Program of China, 2021YFF0502904, YL

National Natural Science Foundation of China, 31925017, 31871087, YL

NIH BRAIN Initiative, 1U01NS113358, 1U01NS120824, YL

FENG Foundation, YL

Data availability statement

The datasets generated during and/or analysed during the current study are available from the corresponding author on reasonable request.

Code availability

The custom-made MatLab code used during the current study are available from GitHub: https://github.com/MieAndersen/NE-oscillations.

References

1. Andrillon T et al. Sleep spindles in humans: insights from intracranial EEG and unit recordings. J Neurosci 31, 17821–34 (2011). [PubMed: 22159098]
2. Fernandez LMJ & Lüthi A Sleep Spindles: Mechanisms and Functions. 10.1152/physrev.00042.2018 (2020) doi:10.1152/PHYSREV.00042.2018.
3. Bonnet MH & Arand DL EEG arousal norms by age. J Clin Sleep Med 3, 271–4 (2007). [PubMed: 17561594]
4. Boselli M, Parrino L, Smerieri A & Terzano MG Effect of age on EEG arousals in normal sleep. Sleep 21, 351–7 (1998). [PubMed: 9646379]
5. Bonnet MH Effect of Sleep Disruption on Sleep, Performance, and Mood. Sleep 8, 11–19 (1985). [PubMed: 3992104]
6. Rauchs G et al. Is there a link between sleep changes and memory in Alzheimer's disease? Neuroreport 19, 1159–62 (2008). [PubMed: 18596620]
7. Landolt HP, Dijk DJ, Achermann P & Borbély AA Effect of age on the sleep EEG: slow-wave activity and spindle frequency activity in young and middle-aged men. Brain Res 738, 205–12 (1996). [PubMed: 8955514]
8. Soltani S et al. Sleep–Wake Cycle in Young and Older Mice. Frontiers in Systems Neuroscience 13, 51 (2019). [PubMed: 31611779]
9. Saper CB, Fuller PM, Pedersen NP, Lu J & Scammell TE Sleep state switching. Neuron 68, 1023–42 (2010). [PubMed: 21172606]
10. Constantinople CM & Bruno RM Effects and Mechanisms of Wakefulness on Local Cortical Networks. Neuron 69, 1061–1068 (2011). [PubMed: 21435553]
11. Aston-Jones G & Bloom FE Activity of norepinephrine-containing locus coeruleus neurons in behaving rats anticipates fluctuations in the sleep-waking cycle. J Neurosci 1, 876–886 (1981). [PubMed: 7346592]
12. Hobson JA, McCarley RW & Wyzinski PW Sleep cycle oscillation: reciprocal discharge by two brainstem neuronal groups. Science 189, 55–8 (1975). [PubMed: 1094539]
13. Eschenko O & Sara SJ Learning-dependent, transient increase of activity in noradrenergic neurons of locus coeruleus during slow wave sleep in the rat: brain stem-cortex interplay for memory consolidation? Cereb Cortex 18, 2596–603 (2008). [PubMed: 18321875]

Author Manuscript Author Manuscript Author Manuscript Author Manuscript

14. Eschenko O, Magri C, Panzeri S & Sara SJ Noradrenergic Neurons of the Locus Coeruleus Are Phase Locked to Cortical Up-Down States during Sleep. Cerebral Cortex 22, 426–435 (2012). [PubMed: 21670101]
15. Carter ME et al. Tuning arousal with optogenetic modulation of locus coeruleus neurons. Nature Neuroscience 13, 1526–1533 (2010). [PubMed: 21037585]
16. Rasmussen K, Morilak DA & Jacobs BL Single unit activity of locus coeruleus neurons in the freely moving cat. I. During naturalistic behaviors and in response to simple and complex stimuli. Brain Res 371, 324–34 (1986). [PubMed: 3697761]
17. Foote SL, Aston-Jones G & Bloom FE Impulse activity of locus coeruleus neurons in awake rats and monkeys is a function of sensory stimulation and arousal. Proc Natl Acad Sci U S A 77, 3033–7 (1980). [PubMed: 6771765]
18. Shouse MN, Staba RJ, Saquib SF & Farber PR Monoamines and sleep: microdialysis findings in pons and amygdala. Brain Research 860, 181–189 (2000). [PubMed: 10727641]
19. Léna I et al. Variations in extracellular levels of dopamine, noradrenaline, glutamate, and aspartate across the sleep-wake cycle in the medial prefrontal cortex and nucleus accumbens of freely moving rats. Journal of Neuroscience Research 81, 891–899 (2005). [PubMed: 16041801]
20. Yamaguchi H, Hopf FW, Li S-B & de Lecea L. In vivo cell type-specific CRISPR knockdown of dopamine beta hydroxylase reduces locus coeruleus evoked wakefulness. Nature Communications 9, 5211 (2018).
21. Rajkowski J, Kubiak P & Aston-Jones G Locus coeruleus activity in monkey: Phasic and tonic changes are associated with altered vigilance. Brain Research Bulletin 35, 607–616 (1994). [PubMed: 7859118]
22. Swift KM et al. Abnormal Locus Coeruleus Sleep Activity Alters Sleep Signatures of Memory Consolidation and Impairs Place Cell Stability and Spatial Memory. Current Biology 28, 3599–3609 (2018). [PubMed: 30393040]
23. Lecci S et al. Coordinated infraslow neural and cardiac oscillations mark fragility and offline periods in mammalian sleep. Science Advances 3, e1602026 (2017). [PubMed: 28246641]
24. Osorio-Forero A et al. Infraslow locus coeruleus activity coordinates spindle rhythms and heart rate to gate fluctuating non-REM sleep substates. bioRxiv 2021.03.08.434399 (2021) doi:10.1101/2021.03.08.434399.
25. Novitskaya Y, Sara SJ, Logothetis NK & Eschenko O Ripple-triggered stimulation of the locus coeruleus during post-learning sleep disrupts ripple/spindle coupling and impairs memory consolidation. Learning and Memory 23, 238–248 (2016). [PubMed: 27084931]
26. Feng J et al. A Genetically Encoded Fluorescent Sensor for Rapid and Specific In Vivo Detection of Norepinephrine. Neuron 102, 745–761 (2019). [PubMed: 30922875]
27. EEG arousals: scoring rules and examples: a preliminary report from the Sleep Disorders Atlas Task Force of the American Sleep Disorders Association. Sleep 15, 173–84 (1992). [PubMed: 11032543]
28. Aston-Jones G & Bloom FE Activity of norepinephrine-containing locus coeruleus neurons in behaving rats anticipates fluctuations in the sleep-waking cycle. J Neurosci 1, 876–886 (1981). [PubMed: 7346592]
29. Gottesmann C The transition from slow-wave sleep to paradoxical sleep: Evolving facts and concepts of the neurophysiological processes underlying the intermediate stage of sleep. Neuroscience and Biobehavioral Reviews 20, 367–387 (1996). [PubMed: 8880730]
30. Krueger JN et al. Amnesia for context fear is caused by widespread disruption of hippocampal activity. Neurobiology of Learning and Memory 175, 107295 (2020). [PubMed: 32822864]
31. Takeuchi T et al. Locus coeruleus and dopaminergic consolidation of everyday memory. Nature 537, 357–362 (2016). [PubMed: 27602521]
32. Mahn M, Prigge M, Ron S, Levy R & Yizhar O Biophysical constraints of optogenetic inhibition at presynaptic terminals. Nat Neurosci 19, 554 (2016). [PubMed: 26950004]
33. de Medeiros MA, Reis LC & Mello LE Stress-induced c-Fos expression is differentially modulated by dexamethasone, diazepam and imipramine. Neuropsychopharmacology 30, 1246–1256 (2005). [PubMed: 15714225]

Author Manuscript Author Manuscript Author Manuscript Author Manuscript

34. Mayers AG & Baldwin DS Antidepressants and their effect on sleep. Hum Psychopharmacol 20, 533–559 (2005). [PubMed: 16229049]
35. Mitchell HA & Weinshenker D Good night and good luck: norepinephrine in sleep pharmacology. Biochem Pharmacol 79, 801–809 (2010). [PubMed: 19833104]
36. Watts A, Gritton HJ, Sweigart J & Poe GR Behavioral/Systems/Cognitive Antidepressant Suppression of Non-REM Sleep Spindles and REM Sleep Impairs Hippocampus-Dependent Learning While Augmenting Striatum-Dependent Learning. (2012) doi:10.1523/JNEUROSCI.0170-12.2012.
37. Porter-Stransky KA et al. Noradrenergic Transmission at Alpha1-Adrenergic Receptors in the Ventral Periaqueductal Gray Modulates Arousal. Biological Psychiatry 85, 237–247 (2019). [PubMed: 30269865]
38. Rudzik F et al. Sleep spindle characteristics and arousability from nighttime transportation noise exposure in healthy young and older individuals. Sleep 41, (2018).
39. Peter-Derex L, Yammine P, Bastuji H & Croisile B Sleep and Alzheimer's disease. Sleep Med Rev 19, 29–38 (2015). [PubMed: 24846773]
40. Scammell TE, Arrigoni E & Lipton JO Neural Circuitry of Wakefulness and Sleep. Neuron 93, 747 (2017). [PubMed: 28231463]
41. Luppi PH, Aston-Jones G, Akaoka H, Chouvet G & Jouvet M Afferent projections to the rat locus coeruleus demonstrated by retrograde and anterograde tracing with cholera-toxin B subunit and Phaseolus vulgaris leucoagglutinin. Neuroscience 65, 119–160 (1995). [PubMed: 7753394]
42. Aston-Jones G, Ennis M, Pieribone VA, Nickell WT & Shipley MT The brain nucleus locus coeruleus: restricted afferent control of a broad efferent network. Science 234, 734–737 (1986). [PubMed: 3775363]
43. Picchioni D et al. Autonomic arousals contribute to brain fluid pulsations during sleep. Neuroimage 249, 118888 (2022). [PubMed: 35017126]
44. Fultz NE et al. Coupled electrophysiological, hemodynamic, and cerebrospinal fluid oscillations in human sleep. Science 366, 628–631 (2019). [PubMed: 31672896]
45. Osorio-Forero A et al. Noradrenergic circuit control of non-REM sleep substates. Current Biology 31, 5009–5023.e7 (2021). [PubMed: 34648731]
46. Gottesmann C The transition from slow-wave sleep to paradoxical sleep: Evolving facts and concepts of the neurophysiological processes underlying the intermediate stage of sleep. Neuroscience and Biobehavioral Reviews 20, 367–387 (1996). [PubMed: 8880730]
47. Purcell SM et al. Characterizing sleep spindles in 11,630 individuals from the National Sleep Research Resource. Nature Communications 2017 8:1 8, 1–16 (2017).
48. Dringenberg HC & Olmstead MC Integrated contributions of basal forebrain and thalamus to neocortical activation elicited by pedunculopontine tegmental stimulation in urethane-anesthetized rats. Neuroscience 119, 839–853 (2003). [PubMed: 12809705]
49. Gervasoni D et al. Effect of chronic treatment with milnacipran on sleep architecture in rats compared with paroxetine and imipramine. Pharmacology Biochemistry and Behavior 73, 557–563 (2002). [PubMed: 12151030]
50. Jones BE The role of noradrenergic locus coeruleus neurons and neighboring cholinergic neurons of the pontomesencephalic tegmentum in sleep-wake states. Progress in Brain Research 88, 533–543 (1991). [PubMed: 1813933]
51. Williams JA & Reiner PB Noradrenaline hyperpolarizes identified rat mesopontine cholinergic neurons in vitro. J Neurosci 13, 3878–3883 (1993). [PubMed: 8103553]
52. Latchoumane C.-F. v, Ngo H.-V. v, Born J & Shin H-S Thalamic Spindles Promote Memory Formation during Sleep through Triple Phase-Locking of Cortical, Thalamic, and Hippocampal Rhythms. Neuron 95, 424–435.e6 (2017). [PubMed: 28689981]
53. Li W, Ma L, Yang G & Gan W-B REM sleep selectively prunes and maintains new synapses in development and learning. Nat Neurosci 20, 427–437 (2017). [PubMed: 28092659]
54. Ribeiro S et al. Novel experience induces persistent sleep-dependent plasticity in the cortex but not in the hippocampus. Front Neurosci 1, 43–55 (2007). [PubMed: 18982118]
55. Giuditta A et al. The sequential hypothesis of the function of sleep. Behavioural Brain Research 69, 157–166 (1995). [PubMed: 7546307]

Author Manuscript Author Manuscript Author Manuscript Author Manuscript

56. Gais S, Rasch B, Dahmen JC, Sara S & Born J The Memory Function of Noradrenergic Activity in Non-REM Sleep. Journal of Cognitive Neuroscience 23, 2582–2592 (2011). [PubMed: 21261452]

57. Rasch B, Pommer J, Diekelmann S & Born J Pharmacological REM sleep suppression paradoxically improves rather than impairs skill memory. Nature Neuroscience 2008 12:4 12, 396–397 (2008).

58. Aghajanian GK & VanderMaelen CP alpha 2-adrenoceptor-mediated hyperpolarization of locus coeruleus neurons: intracellular studies in vivo. Science 215, 1394–6 (1982). [PubMed: 6278591]

59. Washburn M & Moises HC Electrophysiological correlates of presynaptic alpha 2-receptor-mediated inhibition of norepinephrine release at locus coeruleus synapses in dentate gyrus. J Neurosci 9, 2131–40 (1989). [PubMed: 2542486]

60. Hayat H et al. Locus coeruleus norepinephrine activity mediates sensory-evoked awakenings from sleep. Sci Adv 6, eaaz4232 (2020). [PubMed: 32285002]

61. Oe Y et al. Distinct temporal integration of noradrenaline signaling by astrocytic second messengers during vigilance. Nature Communications 11, 471 (2020).

Author Manuscript
Author Manuscript
Author Manuscript
Author Manuscript

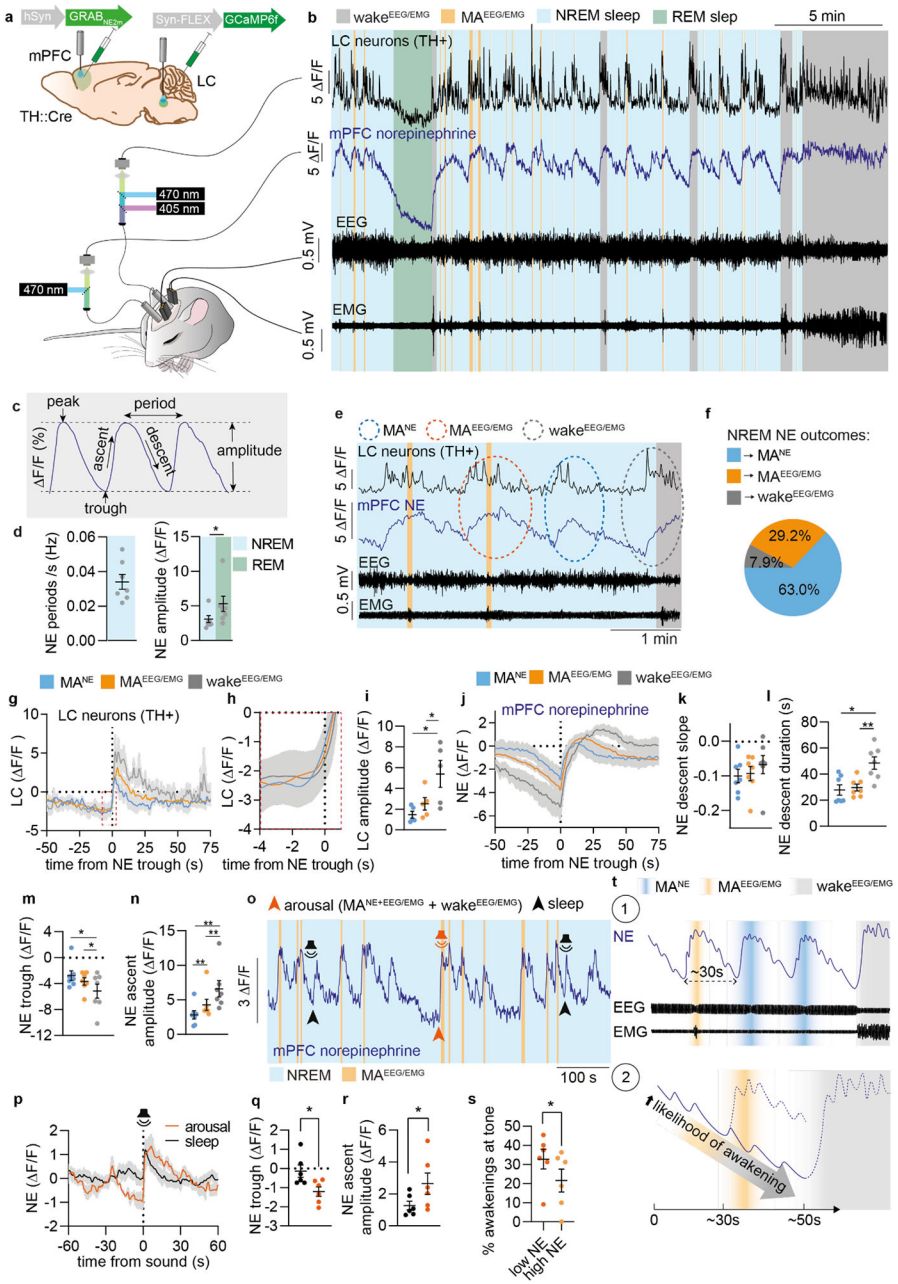

Figure 1. Increased NE descent amplitude primes awakenings over micro-arousals.

a. $GRAB_{NE2m}$ and GCAMP6f were expressed in medial prefrontal cortex (mPFC) and locus coeruleus (LC), respectively, for combined norepinephrine (NE) and LC Ca^{2+} measurements alongside EEG and EMG recordings. **b.** Representative traces of simultaneous recordings with EEG- scored sleep stages. **c.** Terminology used to describe NE oscillations. **d.** Mean NE oscillation frequency and amplitude during NREM and REM sleep (two-tailed paired *t*-test, $P = 0.020$). **e.** Representative traces showing NREM-related NE events associated with micro-arousals accompanied only by EEG and not EMG changes (MA^{NE}), EEG/EMG-defined micro-arousals ($MA^{EEG/EMG}$), or waking. **f.** Percentage of state transition outcome from each NE period. **g.** Mean LC traces aligned to onset of NE ascent. **h.** Zoom-in of mean

Author Manuscript Author Manuscript Author Manuscript Author Manuscript

LC traces (red dotted square in **g**). **i.** Amplitude of LC responses across all state transitions (two-tailed paired *t*-test; $P = 0.09$, MA^{NE} vs $MA^{EEG/EMG}$; $P = 0.02$, MA^{NE} vs wake; $P = 0.04$, $MA^{EEG/EMG}$ vs wake). **j.** Mean NE traces aligned to onset of NE rise at behavioral transitions. **k-n.** Mean slope of NE descent (two-tailed paired *t*-test; $P = 0.55$, NREM vs $MA^{EEG/EMG}$; $P = 0.20$, NREM vs wake; $P = 0.19$, $MA^{EEG/EMG}$ vs wake), NE descent time (two-tailed paired *t*-test; $P = 0.58$, MA^{NE} vs $MA^{EEG/EMG}$; $P = 0.015$, MA^{NE} vs wake; $P = 0.0051$, $MA^{EEG/EMG}$ vs wake), NE trough level (two-tailed paired *t*-test; $P = 0.22$, MA^{NE} vs $MA^{EEG/EMG}$; $P = 0.032$, MA^{NE} vs wake; $P = 0.049$, $MA^{EEG/EMG}$ vs wake), and NE ascent amplitude prior to transitions (two-tailed paired *t*-test; $P = 0.0068$, MA^{NE} vs $MA^{EEG/EMG}$; $P = 0.0021$, MA^{NE} vs wake; $P = 0.0022$, $MA^{EEG/EMG}$ vs wake). **o.** Another batch of animals was exposed to tones during sleep/wake behavior while $GRAB_{NE2m}$ fluorescence was measured as shown in representative trace. Tones during NREM sleep were divided into outcome (sleep or arousal). **p.** Mean NE traces related to tone onset. **q-r.** NE trough level (two-tailed, paired *t*-test; $P = 0.048$) and ascent amplitude (two-tailed paired *t*-test; $P = 0.025$) at tone-induced sleep versus arousal. **s.** NE trough levels prior to each tone was classified as low or high (above or below mean NE trough value prior to all tones), and wakeup rate is shown for each group (two-tailed paired *t*-test; $P = 0.043$). **t.** Schematic summarizing our two main findings on the role of NE in sleep microarchitecture: 1) Regular NE oscillations dictate micro-arousals; 2) Longer periods of NE descent associate with increased probability of awakening. **d-n:** n = 7; **o-s:** n = 6. Data is shown as mean±SEM. $*P < 0.05$, $**P < 0.01$, $***P < 0.001$.

Author Manuscript Author Manuscript Author Manuscript Author Manuscript

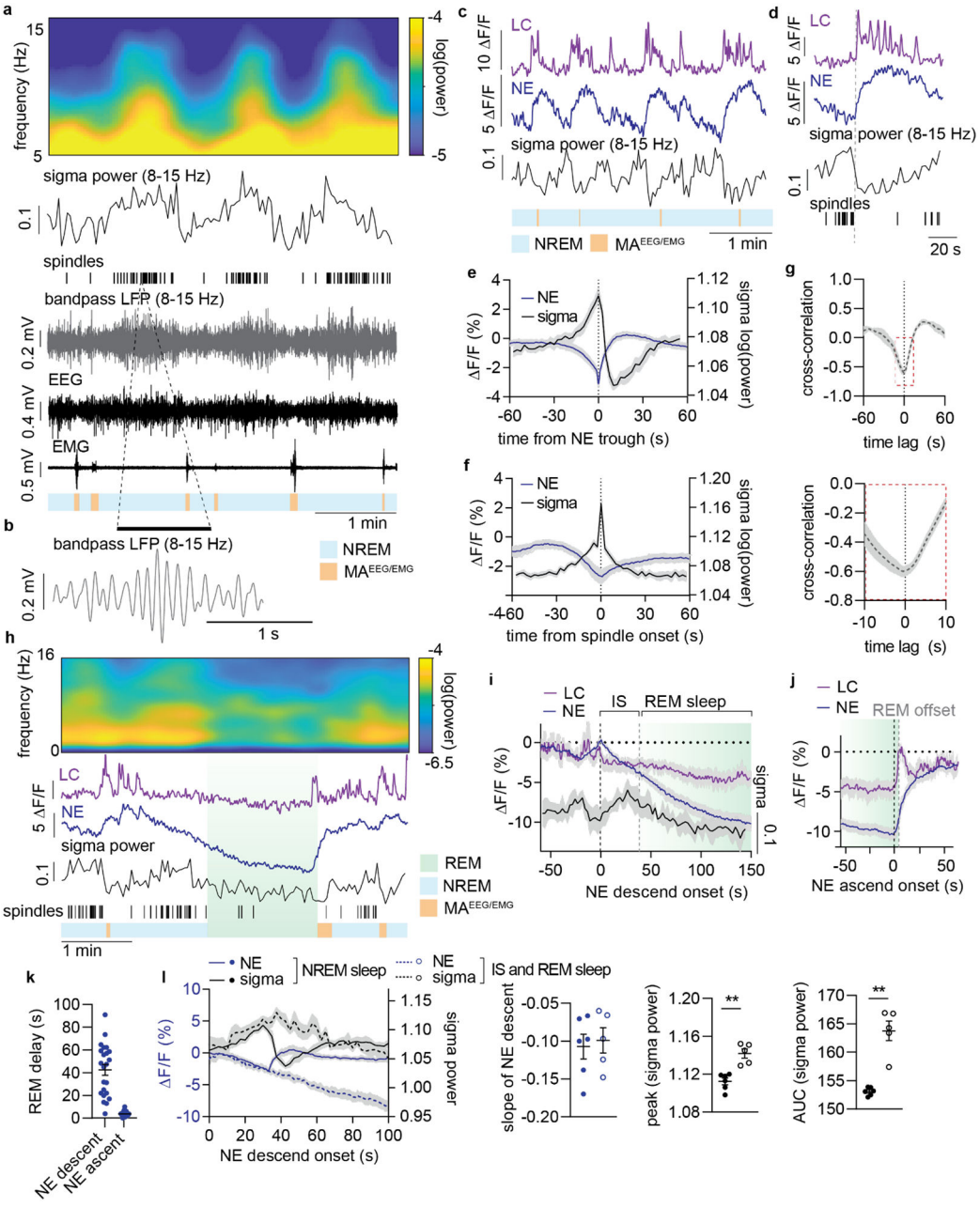

Figure 2. Prolonged NE descent promotes spindle-rich IS and REM sleep transitions.

a. Representative simultaneous surface EEG and depth local field potential (LFP) recordings showing the correlation between LFP-based spindle detection and EEG-based sigma power. Displayed are EEG power spectrogram, EEG-based sigma power, LFP-based spindle occurrences, 8-15 Hz bandpass filtered LFP, raw EEG and EMG, and color-coded sleep phases. **b.** Zoom-in of 8-15 Hz bandpass filtered LFP showing a representative spindle. **c.** Representative traces from simultaneous measurements of locus coeruleus (LC) and norepinephrine (NE) during NREM sleep and their association with sigma power. **d.** Representative LC and NE traces as well as sigma power and spindle occurrences upon NE ascent. **e.** Mean NE and sigma power traces aligned to NE trough during NREM

Author Manuscript Author Manuscript Author Manuscript Author Manuscript

sleep. **f.** Mean NE and sigma power traces aligned to spindle onset during NREM sleep. **g.** Cross-correlation between sigma power and NE level based on 10 min NREM sleep epochs. Bottom: zoom-in to illustrate time lag. **h.** Representative recordings covering REM sleep transitions (REM sleep>150 s in duration) showing EEG power spectrogram, LC and NE traces, sigma power, spindle occurrences and color-coded sleep phases. **i.** Mean LC and NE activity, and sigma power from NE descent onset preceding REM onset. Mean onset of REM sleep is displayed . The period from NE descent onset until REM sleep onset is marked as intermediate state (IS) sleep. **j.** Mean LC and NE activity during REM sleep aligned to the onset of NE ascent preceding REM sleep offset. Mean REM sleep offset is marked. **k.** Mean delay from NE descent onset to REM sleep onset and from NE ascent to REM sleep offset (23 REM sleep occurrences across n = 5). **l.** Mean NE and sigma power during NREM sleep versus IS-REM sleep from the onset of NE descent; slope of NE descent for NREM and IS sleep (two-tailed, paired *t*-test; $P = 0.89$); increase in sigma power peak (two-tailed, paired *t*-test; $P = 0.006$) and area under the curve (AUC) (two-tailed, paired *t*-test; $P = 0.005$) NREM and IS-REM sleep. Significance was calculated by means of paired t-test. n = 6 (NREM); n = 5 (IS-REM). Data is shown as mean±SEM. $^{**}P < 0.01$.

Author Manuscript Author Manuscript Author Manuscript Author Manuscript

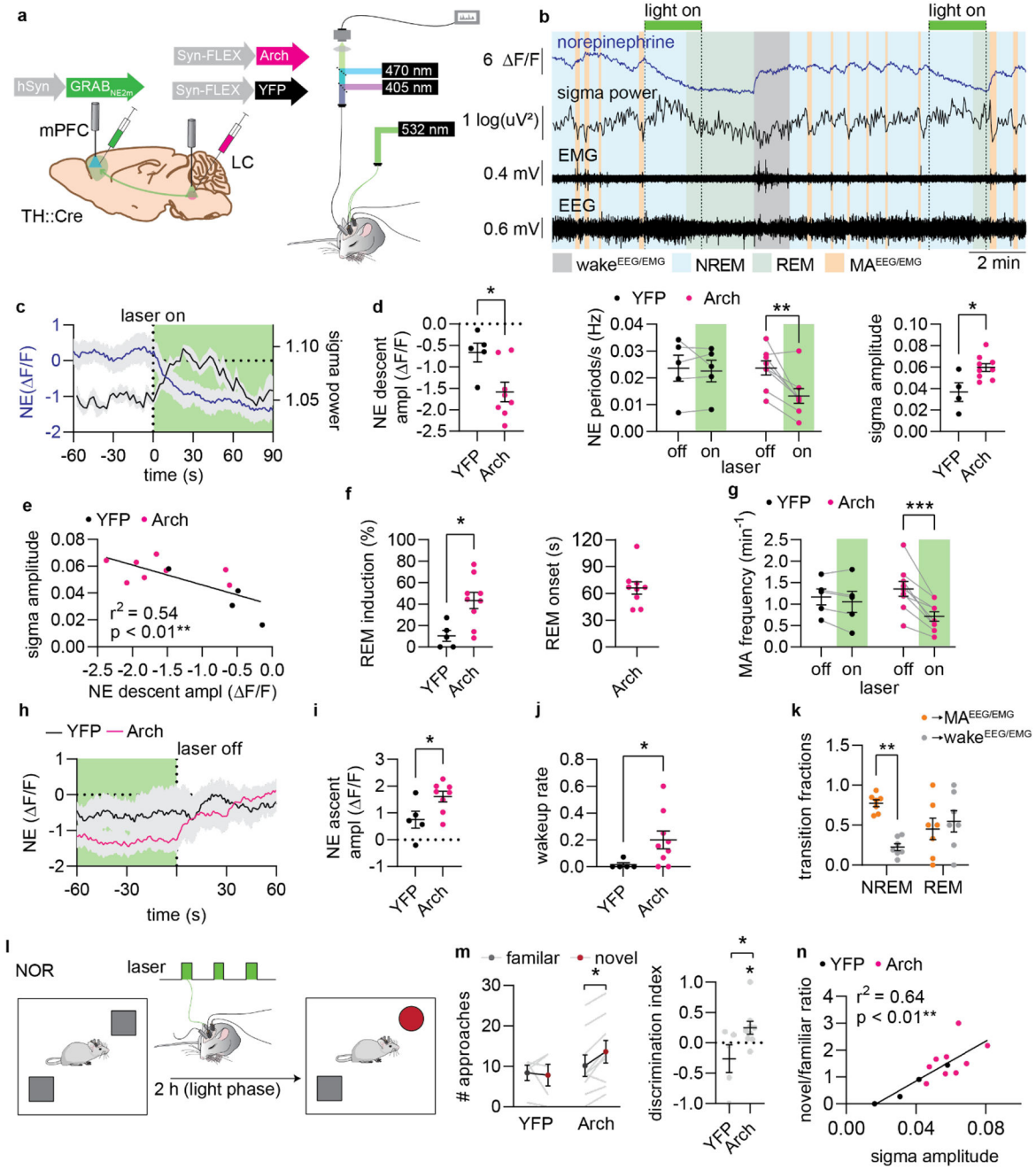

Figure 3. Optogenetic suppression of LC induces IS-REM sleep sequences and improves memory.

a. Arch, was expressed in LC, while $GRAB_{NE2m}$ was expressed in mPFC. Green laser light was delivered to LC during combined fiber photometry and EEG/EMG recordings. **b.** Example traces showing the effects of 2 min optogenetic suppression of LC on norepinephrine levels and sigma power. **c.** Mean NE and sigma power traces aligned to laser stimulation onset in Arch-expressing animals. **d.** NE descent amplitude induced by laser onset during NREM sleep (left) (two-tailed unpaired *t*-test, $P = 0.020$), NE oscillation frequency for laser off- and on-periods (middle) (2-way repeated measures ANOVA with

Author Manuscript Author Manuscript Author Manuscript Author Manuscript

Šídák's multiple comparison post hoc test, $P = 0.92$ YFP; $P = 0.0016$, Arch), and mean amplitude of sigma response after laser onset (right) (two-tailed unpaired *t*-test, $P = 0.015$). **e.** Correlation between sigma amplitude and NE change in response to laser stimulation (linear regression). **f.** Percentage of 2 min laser stimulations resulting in REM transition (left) (two-tailed unpaired *t*-test, $P = 0.011$). Mean time from laser onset before REM onset (right). **g.** Frequency of EEG/EMG-defined micro-arousals (MA) during optogenetic LC suppression (2-way repeated measures ANOVA with Šídák's multiple comparison post hoc test, $P = 0.60$, YFP; $P < 0.0001$, Arch). **h.** Mean NE traces aligned to laser stimulation offset. **i.** NE ascend amplitude after laser offset (two-tailed unpaired *t*-test, $P = 0.033$). **j.** The wakeup rate within 15 s of laser offset (one-tailed Mann-Whitney test, $P = 0.018$). **k.** Outcome of sleep termination from NREM and REM sleep (animals from Fig. 1-2, 2-way repeated measures ANOVA with Šídák's multiple comparison post hoc test, $P = 0.0013$, NREM, $P = 0.75$, REM). **l.** Animals were subjected to novel object recognition and allowed to sleep for two hours with laser stimulations between encoding and recall. **m.** Number of approaches to novel and familiar objects (2-way repeated measures ANOVA with Šídák's multiple comparison post hoc test, $P = 0.91$ YFP; $P = 0.023$, Arch) and discrimination index (one-sample *t*-test, $P = 0.32$ YFP; $P = 0.047$, Arch, two-tailed unpaired *t*-test, $P = 0.038$). **n.** Correlation between approach ratio and mean sigma response to laser stimulations during sleep (linear regression). n = 9 Arch, 5 YFP. Data is shown as mean±SEM. $*P < 0.05$, $**P < 0.01$, $***P < 0.001$.

Author Manuscript Author Manuscript Author Manuscript Author Manuscript

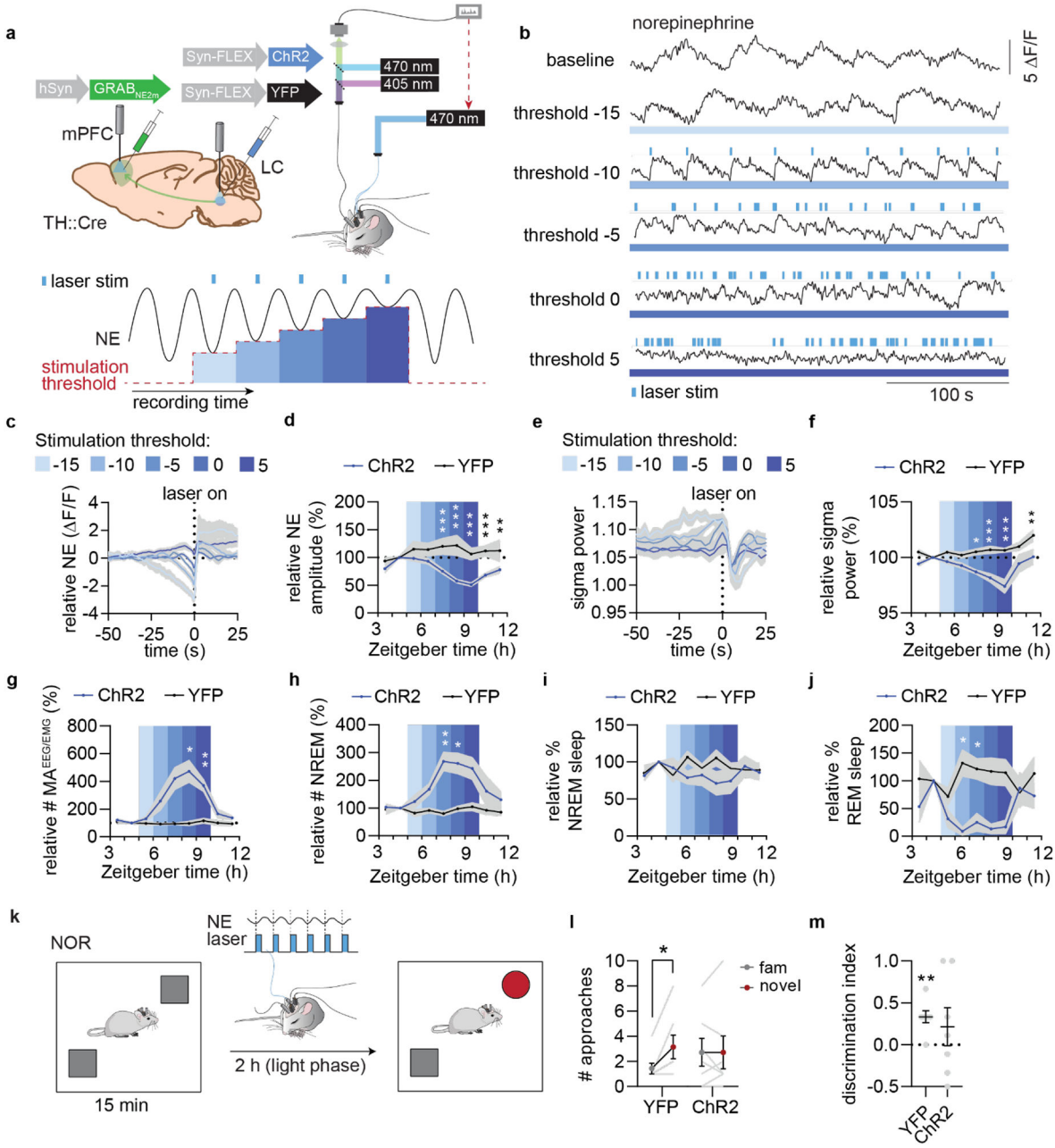

Figure 4. Optogenetic reduction of NE amplitude reduces sigma activity and disrupts memory.

a. Top: ChR2, was expressed in LC, while $GRAB_{NE2m}$ was expressed in mPFC. Blue laser light was delivered to LC during combined fiber photometry and EEG/EMG recordings. Bottom: 2 h baseline recording was followed by 5 periods lasting 1 h with increasing NE thresholds for laser stimulations, followed by a 2 h stimulation-free period. Llaser stimulations were triggered when real-time ΔF/F (%) calculations of NE levels went below the threshold. . **b.** Example traces from each stimulation period is shown with triggered laser stimulations. **c.** Normalized mean NE traces leading up to laser onset for each stimulation threshold. **d.** Mean relative NE amplitude during NREM sleep across each stimulation paradigm (2-way repeated measures ANOVA with Šídák's multiple comparison post hoc

Author Manuscript Author Manuscript Author Manuscript Author Manuscript

test, $P = 0.0006$, threshold −5; $P < 0.0001$, threshold 0; $P < 0.0001$, threshold 5; $P = 0.0008$, washout 1; $P = 0.0079$, washout 2). **e.** Mean sigma power leading up to laser stimulation for each threshold. **f.** Mean relative sigma power during NREM sleep across stimulation paradigms (2-way repeated measures ANOVA with Šídák's multiple comparison post hoc test, $P = 0.012$, threshold −5; $P = 0.0001$, threshold 0; $P < 0.0001$, threshold 5; $P = 0.0055$, washout 2). **g-h.** Number of micro-arousals ($MA^{EEG/EMG}$) per minute spent in NREM sleep (2-way repeated measures ANOVA with Šídák's multiple comparison post hoc test, $P = 0.028$, threshold 0; $P = 0.0064$, threshold 5) and NREM sleep bouts per hour (2-way repeated measures ANOVA with Šídák's multiple comparison post hoc test, $P = 0.0090$, threshold −5; $P = 0.037$, threshold 0) during each stimulation paradigm. **i-j.** Percent time spent in NREM (2-way repeated measures ANOVA with Šídák's multiple comparison post hoc test) and REM sleep (2-way repeated measures ANOVA with Šídák's multiple comparison post hoc test, $P = 0.024$, threshold −10; $P = 0.025$, threshold −5) across stimulation paradigms. **k.** Animals were subjected to novel object recognition and stimulated using the threshold=0 paradigm for 2 h between memory encoding and recall. **l.** Number of approaches to familiar and novel objects (2-way repeated measures ANOVA with Šídák's multiple comparison post hoc test, $P = 0.022$ YFP; $P > 0.99$, ChR2). **m.** Discrimination index based on number of approaches (one sample *t*-test, $P = 0.0038$, YFP; $P = 0.38$, ChR2; two-tailed unpaired *t*-test, $P = 0.63$). n = 7 ChR2, 7 YFP. Data is shown as mean±SEM. *P< 0.05, **P< 0.01, ***P< 0.001.

Author Manuscript Author Manuscript Author Manuscript Author Manuscript

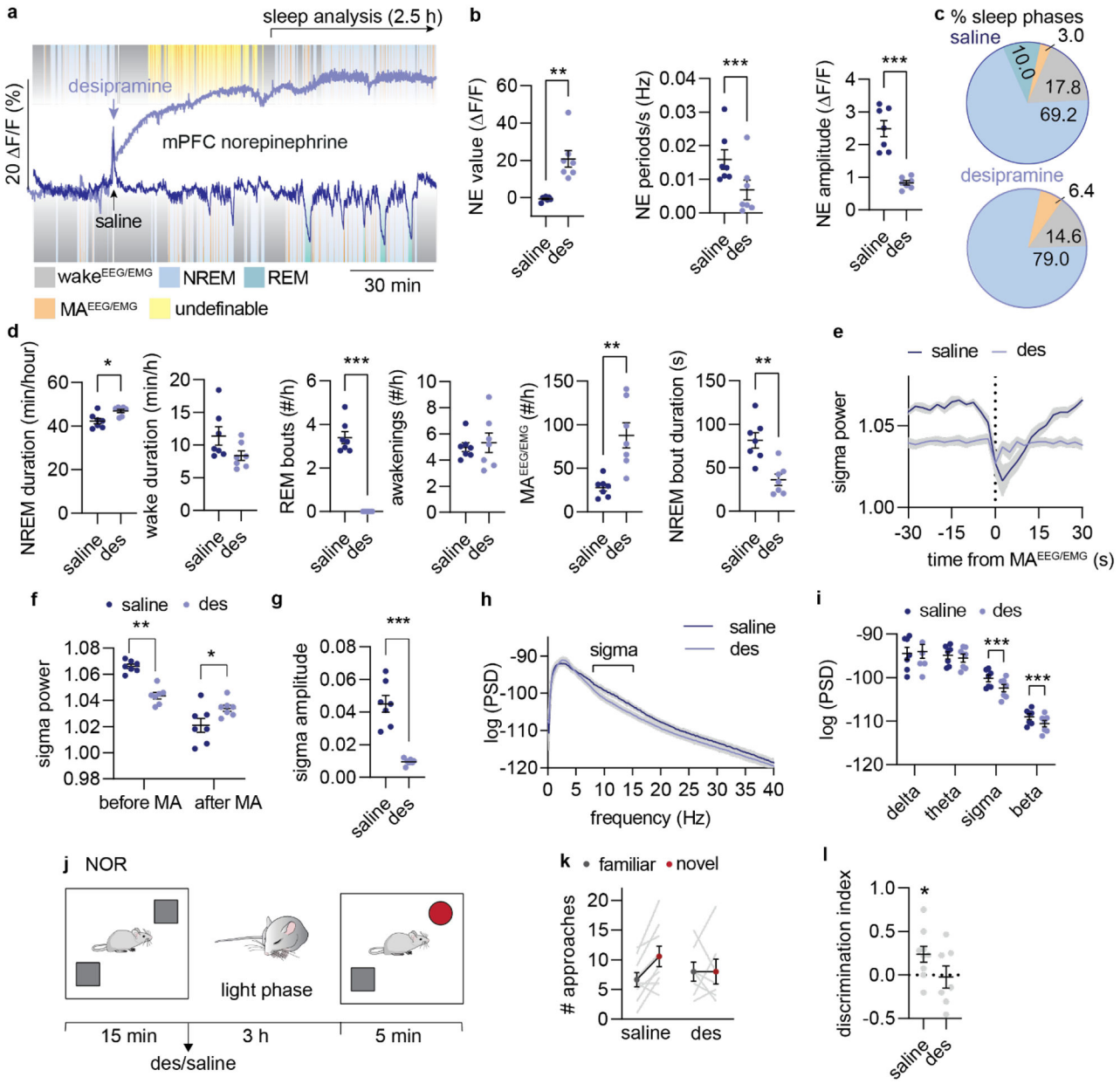

Figure 5. Pharmacological reduction of NE amplitude promotes micro-arousal and compromises memory.

a. Mice were administered with saline or desipramine (des, 10 mg/kg, i.p.) during the light phase and allowed to sleep for 3.5 hrs. 3 days after, treatment was reversed. Analysis was done on 1-3.5 h period after administration. **b.** Effect of desipramine on mean NE value (two-tailed paired *t*-test, $P = 0.0026$), NE oscillation frequency (two-tailed paired *t*-test, $P = 0.0004$), and NE amplitude during NREM sleep (two-tailed paired *t*-test, $P = 0.0003$). **c.** Mean distribution of % time spent in NREM sleep, REM sleep, wakefulness and micro-arousals. **d.** Time spent in NREM sleep (two-tailed paired *t*-test, $P = 0.030$) and wake (two-tailed paired *t*-test, $P = 0.64$), number of REM bouts (two-tailed paired *t*-test, $P < 0.0001$), wake bouts (two-tailed paired *t*-test, $P = 0.70$), micro-arousals (two-tailed paired

Author Manuscript Author Manuscript Author Manuscript Author Manuscript

t-test, $P = 0.0041$), and mean duration of NREM sleep bouts (two tailed paired *t*-test, $P = 0.0029$). **e.** Mean sigma power traces aligned to NREM-to-MA$^{EEG/EMG}$ transition. **F.** Mean sigma power before and after NREM-to-MA$^{EEG/EMG}$ transition (2-way repeated measures ANOVA with Šídák's multiple comparison post hoc test, $P = 0.0024$, before; $P = 0.031$, after). **g.** Mean sigma power amplitude reduction across NREM-to-MA$^{EEG/EMG}$ transition (two-tailed paired *t*-test, $P = 0.0007$). **h-i.** Power spectral densities during NREM sleep and mean power spectral densities across frequency bands (2-way repeated measures ANOVA with Šídák's multiple comparison post hoc test, $P = 0.72$, delta; $P = 0.10$, alpha; $P = 0.0003$, sigma; $P < 0.0001$, beta). **j.** In a separate experiment, mice were subjected to novel object recognition (NOR) during their light phase and administered with desipramine or saline immediately after the encoding phase. Mice were allowed to sleep for three hours before the recall phase. **k.** Number of approaches towards novel versus familiar object during recall . **l.** Discrimination index for novel versus familiar object (one-sample *t*-test, $P = 0.032$, saline; $P = 0.86$, des; two-tailed unpaired *t*-test, $P = 0.11$). n = 7 (**a-i**), n = 7 des, 9 saline (**j-l**). Data is shown as mean±SEM. $*P < 0.05$, $**P < 0.01$, $***P < 0.001$.

Author Manuscript Author Manuscript Author Manuscript Author Manuscript

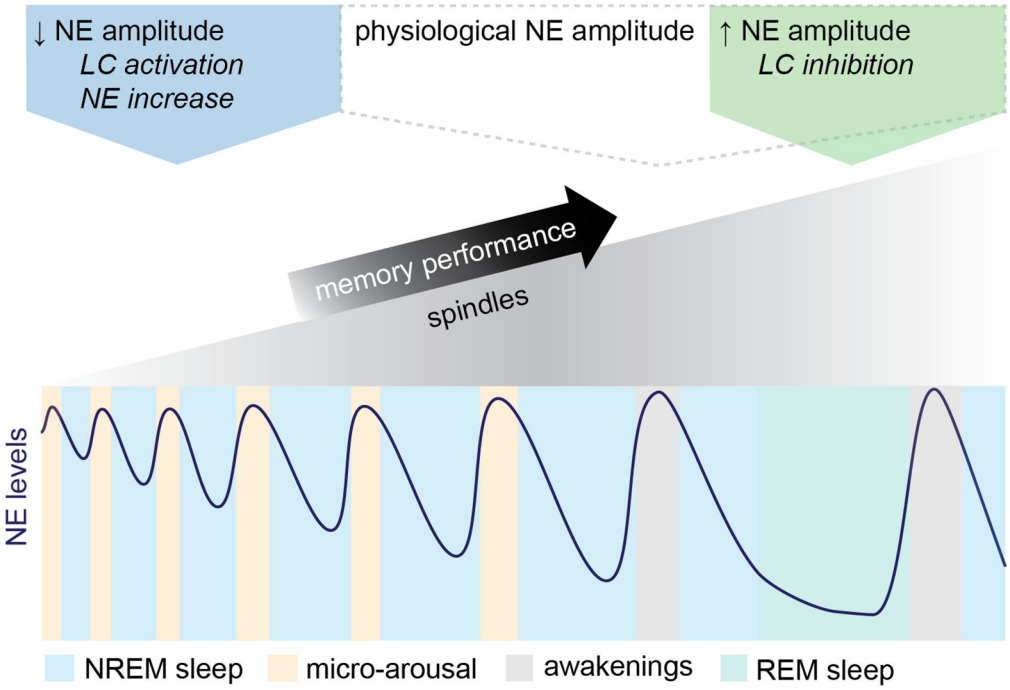

Figure 6. Model diagram: NE amplitude defines the memory restorative properties of sleep.

This diagram depicts NE amplitude changes during normal sleep micro-architecture and LC-NE manipulations: Sleep is characterized by infraslow ~0.02 Hz NE oscillations and the oscillatory amplitude determines both behavioral arousal and the amount of sleep spindles and spindle-rich IS-REM sleep sequences. Reducing NE oscillation amplitude by NE reuptake inhibition or optogenetic activation increases micro-arousals at the cost of spindle-rich sleep needed for memory consolidation. In contrast, augmenting NE amplitude by optogenetic inhibition favors a sleep composition with more frequent spindle-rich ISand REM sleep transitions resulting in improved memory performance despite increased incidents of awakenings.